Transactions of the Canadian Society for Mechanical Engineering

OPEN ACCESS | Research Article

Thermodynamic performance of an ejector–compressor enhanced diffusion–absorption refrigeration system for cement kiln waste heat recovery

Baby-Jean Robert Mungyeko Bisulandu[a,b], Marcel Tsimba Mboko[c], Lucien Mbozi Mbozi[c], Daniel R. Rousse[b], and Adrian Ilinca[b]

[a]Institut de Recherche Futuris – Futuris Research Institute (InReF), OEFC & Institut National du Bâtiment et des Travaux Publics (INBTP), Département de Génie-Rural, B.P. 4731 Kinshasa, DR Congo; [b]Département de Génie Mécanique, École de Technologie Supérieure, 1100 Rue Notre-Dame Ouest, Montréal, QC H3C 1K3, Canada; [c]Département d'Electromécanique, Faculté Polytechnique, Université Président Joseph Kasa-Vubu, B.P. 314 Boma, Kongo Central, DR Congo

Corresponding author: **Adrian Ilinca** (email: adrian.ilinca@etsmtl.ca)

Trans. Can. Soc. Mech. Eng. Downloaded from cdnsciencepub.com by Ecole de technologie superieure on 09/25/26

Abstract

The growing scarcity and rising costs of fossil fuels are accelerating the global transition toward energy-efficient, low-emission industrial systems. Cement plants reject large amounts of thermal energy through exhaust gases, offering an opportunity for heat recovery. This study investigates the thermodynamic performance of a diffusion–absorption refrigeration (DAR) system enhanced with an ejector and a compressor (DAR-EC) and powered by residual heat from a cement kiln. The system is modelled using the M2EP framework (mass, energy, exergy, and performance) and optimized through a particle swarm algorithm. The particle swarm optimization algorithm identifies optimal pressure and concentration levels that maximize coefficient of performance, subject to constraints on the low-temperature heat source. The working fluid is a ternary H_2O–NH_3–H_2 mixture, enabling continuous circulation between the evaporator and absorber. Integrating the ejector and compressor increases the operating pressure at the evaporator outlet and the absorber inlet, thereby improving cycle performance. A sensitivity analysis to temperature, concentration, and pressure variations is performed. Results show that the DAR-EC configuration significantly increases the cooling capacity and raises the coefficient of performance from 0.27 (DAR) to 0.49 (DAR-EC). Exergy analysis additionally reveals that generator and absorber irreversibilities dominate system losses. The model is validated against published data and demonstrates its suitability for industrial heat-recovery applications. The findings provide a decision-support basis for implementing DAR-EC systems to valorize waste heat. Given that this model uses a water-ammonia mixture, the heat source temperature must be between 80 and 200 °C.

Key words: thermodynamic performance, DAR cycle, ejector–compressor, ammonia–water, waste heat recovery, heating system

1. Introduction

The depletion and rising cost of fossil fuels have intensified global efforts toward an energy transition in which renewable and low-emission technologies play a central role. The surge in energy consumption is closely tied to the heightened exploitation of natural resources, many of which are non-renewable and contribute to significant environmental imbalances when extracted. Industrial facilities are now exploring thermal systems capable of recovering waste heat across multiple temperature levels without additional fuel consumption. Among high-temperature industries, the cement sector is particularly notable: exhaust gases from cement kiln chimneys typically reach around 250 °C, making it one of the most significant sources of industrial heat loss worldwide. The steel industry also generates substantial amounts of high-temperature exhaust gases with significant heat recovery potential. According to Atashbozorg et al. (2022), it ranks second among industrial sectors in terms of recoverable waste heat, as large quantities of excess thermal energy are generated and dissipated due to inadequate energy efficiency policies.

Concurrently, the refrigeration sector is shifting toward more sustainable cooling technologies. Absorption-based refrigeration systems have attracted renewed interest due to their ability to operate using low-grade heat sources and environmentally benign working fluids. The concept of the absorption machine dates to 1859, stemming from the pioneering work of Ferdinand Carré, who patented the technology that year. In contemporary times, the global push for energy transition, a policy aimed at promoting the adoption of environmentally friendly, less polluting green energies significantly advocates that the refrigeration sector embrace

Trans. Can. Soc. Mech. Eng. Downloaded from cdnsciencepub.com by Ecole de technologie superieure on 09/25/26

sustainable systems, mainly through the widespread adoption of absorption refrigeration machines. As noted by Asfand and Bourouis (2015), increasing energy scarcity is expected to further stimulate the development of absorption refrigeration systems, as they can effectively utilize renewable heat sources and natural refrigerants with minimal environmental impact. Numerous absorption configurations have been developed and deployed worldwide, and ongoing research focuses on optimizing system components, including absorbers, generators or boilers, heat sources, condensers, evaporators, auxiliary heat exchangers, and optional pumps, as well as on hybrid configurations combining absorption and compression processes. As a result, absorption technologies are now considered highly relevant for air-conditioning and preservation applications (Chua et al. 2002; Zohar et al. 2005; Karamangil et al. 2010; Starace and De Pascalis 2013; Adjibade et al. 2017; Ezgi and Bayrak 2020).

A substantial body of literature has focused on diffusion–absorption refrigeration (DAR) systems powered by various heat sources. Dhindsa (2021) investigated suitable energy sources for thermochemical solar absorption systems and demonstrated the feasibility of operating DAR cycles using renewable energy. Alcântara et al. (2022) developed a mathematical model for $NH_3/LiNO_3$ absorption coolers, highlighting the critical role of rectification in preventing water carryover and ensuring stable evaporator operation. In the absence of a rectifier, water condensation and accumulation in the evaporator degrade performance. Garma et al. (2025) experimentally studied a DAR system using a low-global warming potential (GWP) working pair (R600/*n*-nonane/helium), achieving an evaporator temperature of −10 °C with a generator temperature of 140 °C. Harraz et al. (2025) employed molecular design tools to identify optimal organic working fluids for solar-driven DAR cycles. Additional studies have explored DAR systems integrated with photovoltaic solar energy.

Further studies have examined the integration of DAR systems with photovoltaic solar energy. Rady et al. (2025) demonstrated a PV-driven DAR system achieving evaporator temperatures between 3.5 and 9.5 °C with a coefficient of performance (COP) of 0.055. Freeman and Markides (2024*a*, 2024*b*) proposed a semi-empirical solar-powered DAR system for rural applications in India, reporting a COP of 0.25 at an operating pressure of 14 bar. To improve the performance of DAR systems, the incorporation of ejectors and/or compressors has proven particularly effective. Consequently, recent research has increasingly focused on hybrid absorption–ejector–compression configurations. These systems typically operate at three pressure levels: the evaporator pressure of the refrigerant vapour, an intermediate pressure reached after the isentropic compression and corresponding to the absorber operating pressure, and the condensing pressure governing the condenser and generator (Lounissi et al. 2017).

Siddique et al. (2025) evaluated four cascade refrigeration configurations to provide efficient low-temperature cooling while reducing energy consumption. Addressing the limitations of conventional systems for exploiting high-temperature waste heat, they integrated a vapour-compression refrigeration (VCR) system with an ejector into absorption refrigeration cycles equipped with a refrigerant heat exchanger. This hybridization significantly improved performance, increasing the COP by approximately 18% and 14% compared with a conventional double-effect compression–absorption cycle.

Dhahi Gharir and Farshi (2023) investigated a double-ejector absorption refrigeration cycle, reporting a COP enhancement of up to 56.8% and an exergy efficiency of 22.5%. Similarly, Khalili and Garousi Farshi (2020) designed and analyzed an absorption refrigeration system incorporating two multi-pressure ejectors, achieving significant improvements in both COP and exergy efficiency compared with systems without ejectors.

Vereda et al. (2012) developed a steady-state numerical model of an ejector-assisted absorption refrigerator system to analyse the influence of ejector geometry on cycle performance and to identify suitable heat-source temperature ranges. In such configurations, the ejector entrains refrigerant vapour from the evaporator and increases the absorber pressure without additional mechanical energy input (see Fig. 1).

Dennis and Garzoli (2011) employed a variable-geometry ejector coupled with a cold-storage system to enhance the solar fraction in solar-cooling applications, thereby improving system efficiency while reducing the required solar collector surface area. Van Nguyen et al. (2020) further investigated the performance of variable-geometry ejectors in small-scale solar air-conditioning systems, aiming to overcome the limitations of fixed-geometry ejectors.

More advanced hybrid absorption–compression configurations have also been proposed. In addition to conventional absorption systems, the literature reports several studies on cascade-connected absorption refrigeration machines (He et al. 2019; Nabil et al. 2023; Walid Faruque et al. 2023; Kayes et al. 2025). He et al. (2019) improved the performance of a conventional solar absorption–compression cascade refrigeration system by integrating an air-cooled vapor compression refrigeration (ACR) cycle. The combined system comprises a solar-driven single-effect absorption refrigeration unit and an electrically powered dual-source vapor compression refrigeration (EDCR) unit, resulting in improved overall efficiency and extended solar energy utilization. The coupled ACR–EDCR configuration reliably satisfies cooling and heating demands under varying operating conditions.

Chen et al. (2016) proposed an absorption/absorption–compression refrigeration configuration with a wide operating range, aimed at enhancing thermal energy utilization in absorption systems subject to large temperature variations or multiple sources. Peng et al. (2022) developed a hybrid absorption–compression cooling system incorporating parallel subcooling and recooling to address the mismatch between small-scale heat sources and large cooling demands. In a related study, Asensio-Delgado et al. (2022) analyzed hybrid compression–absorption refrigeration cycles using low-GWP hydrofluorocarbon refrigerants or hydro-fluoro-olefin refrigerants/ionic-liquid working pairs, demonstrating that compression–absorption refrigeration systems maintain superior performance even at reduced generator temperatures. A comparative summary of the main absorption and hybrid

Fig. 1. (*a*) Conventional absorption refrigeration cycle and (*b*) ejector–absorption refrigeration cycle. Reprinted from Vereda et al. (2012) with permission from Elsevier.

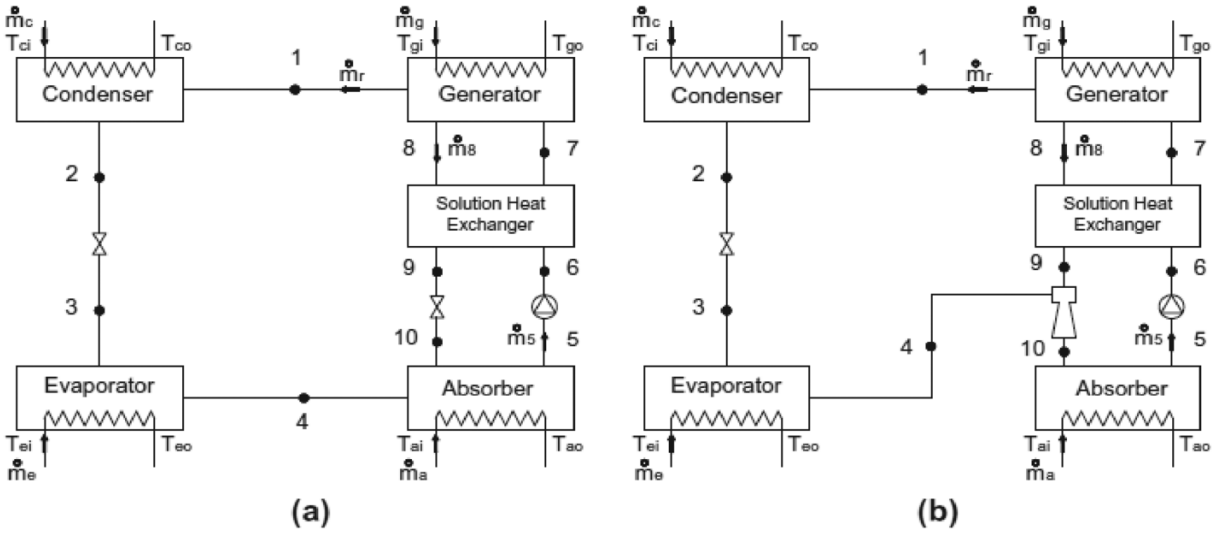


Table 1. Comparison of different absorption machines (Mungyeko Bisulandu et al. 2023).

Types of refrigeration	Pressure level	Advantages	Disadvantages
DAR	Level 1	• Passive operation (Harraz et al. 2019). • Silent Operation (Yildiz et al. 2014; Harraz et al. 2019). • Reliable system (Yildiz et al. 2014). • No vibration. • Long life and low maintenance. • Low investment cost. • The system can be powered by different energy sources: electricity, sun, LPG, and waste heat (Yildiz et al. 2014).	• Low cooling capacity of the DAR system (The cooling capacity of the DAR system is low, not only because the presence of the auxiliary gas inside the evaporator reduces the mass flow of the refrigerator in the system, but also because the heat loss to the ambient in the rectifier cannot be negligible (Yildiz et al. 2014))
DPAR or ARS	Level 2	• Requires a small amount of energy to pump the liquid (Papadopoulos et al. 2019). • Ability to produce cooling from low-temperature heat sources (Papadopoulos et al. 2019). • Cold production does not require high input shaft power (Garousi Farshi et al. 2011). • Possibility of using low-quality heat (solar thermal, fuel cells, waste heat, geothermal energy, etc.) (Garousi Farshi et al. 2011).	• Low yield (Garousi Farshi et al. 2011; Jiang et al. 2022). • Limitation of the temperature of the heat source used (Garousi Farshi et al. 2011). • Limitations of small capacity applications (Asfand and Bourouis 2015).
ACR	Level 3	• Acceptable energy efficiency (Chen et al. 2016; Garousi Farshi et al. 2011; He et al. 2019; Peng et al. 2022).	• Pumping liquid requires a large fraction of energy (Papadopoulos et al. 2019).
EAR	Level 3	• Increased pressure at the absorber (Vereda et al. 2012).	–

Note: DAR, diffusion–absorption refrigeration; DPAR, dual-pressure absorption-refrigeration; ARS, absorption refrigeration systems; ACR, air-cooled vapor compression refrigeration; EAR, ejector-absorption refrigeration.

refrigeration cycles discussed in the literature is provided in Table 1.

It is important to note that although absorption refrigeration systems (ARS) can operate with low-temperature heat sources, they still face significant temperature-related limitations that hinder achieving optimal COP values. This constraint reinforces the need for continued optimization of ARS technologies (see Zhang et al. 2022).

Despite the abundance of work on absorption systems and hybrid configurations, the literature remains primarily focused on improving COP and exergy efficiency, at the expense of an in-depth analysis of industrial integration. Studies on diffusion–absorption systems remain limited and are often restricted to experimental cases or low-power solar sources. Furthermore, detailed modelling of key components, particularly the ejector, is often simplified or decoupled from the overall cycle behaviour. The specific influence of ternary mixtures, particularly $NH_3/H_2O/H_2$, on ejector performance remains insufficiently explored. In addition, a few studies propose models for recovering high-temperature waste heat

Trans. Can. Soc. Mech. Eng. Downloaded from cdnsciencepub.com by Ecole de technologie superieure on 09/25/26

Trans. Can. Soc. Mech. Eng. Downloaded from cdnsciencepub.com by Ecole de technologie superieure on 09/25/26

from heavy industrial sectors. Finally, techno-economic aspects and large-scale industrial feasibility are still rarely addressed systematically.

In view of the research gaps mentioned above, this article proposes to study the thermodynamic performance of diffusion absorption refrigeration cycles using the residual heat from hot gases emitted from a cement kiln chimney. First, the study focuses on the DAR configuration; second, on the improved DAR configuration equipped with an ejector and a compressor, the diffusion–absorption refrigeration system enhanced with an ejector and a compressor (DAR-EC) system. In both configurations, the residual heat from a cement kiln's exhaust gases, recovered by high-performance heat exchangers, is used to heat the ammonia solution in the generator. A comparison between the performance of the DAR-EC system and that of the conventional DAR cycle presented in previous work (Mungyeko Bisulandu et al. 2024) is provided in the "Results and discussion" section. The originality of this study lies in its in-depth analysis of industrial integration, particularly in the cement industry, and its focus on the recovery of high-temperature waste heat from heavy industry. It also examines the design of DAR and DAR-EC configurations specifically adapted to low-cost heat recovery from high- and low-temperature streams in a cement rotary kiln.

This article is structured as follows: first, a description of the system is provided, detailing how the two cycles studied work and explaining and justifying the choice of DAR type. Next, an analysis and description of the working fluid are presented to understand its behaviour during saturation evaporation, safety considerations (particularly in the event of leaks or accidental releases), and its GWP. Section 4 discusses pressure and concentration limitations in RAS cycle installations. Next, a model of the DAR and DAR-EC systems is presented. This begins by presenting the data required for the simulation, the M2EP (mass, energy, exergy, and performance) method, a description of the application of the particle swarm optimisation (PSO) algorithm, assumptions, and thermodynamic equations for the ejector. In Section 6, the model's results are presented, analysed, and discussed. A comparison based on performance parameters between DAR and DAR-EC is also presented. To validate the results of this article, a model validation section is added that compares this work's results with those in the literature. Finally, a conclusion and outlook section rounds off this work.

2. Materials and methods

2.1. System description

This study focuses on the thermodynamic performance of a DAR system equipped with an ejector and a compressor, referred to as the DAR-EC configuration. The system utilizes residual hot gases at 109 °C originating from the cogeneration circuit of a Kalina cycle. These gases supply the thermal energy required at the generator to heat the water–ammonia ($H_2O + NH_3$) working solution and initiate vaporization.

The analysis also includes a performance comparison with the DAR system presented in our previous work (Mungyeko Bisulandu et al. 2024). The baseline DAR configuration described by Mazouz et al. (2014) is modified here by integrating an additional compressor and an ejector. The resulting DAR-EC system consists of the following main components: a rectifier, a condenser, an absorber, an evaporator, a compressor, an ejector, two heat exchangers (the gas heat exchanger, GHX, and the solution heat exchanger, SHX), and a generator designed as two externally heated coaxial tubes.

In the generator, the inner tube functions as a bubble pump, receiving heat indirectly from the annular flow surrounding it, and acts similarly to a boiler. The supplied heat, $\dot{Q}_{gen}$, enables partial desorption of ammonia from the rich solution originating from the absorber. The resulting ammonia vapour is subsequently purified in the rectifier through partial condensation of the remaining water vapour, rejecting heat $\dot{Q}_{rec}$. The nearly pure ammonia then condenses in the condenser, releasing heat $\dot{Q}_{cond}$ to the surroundings.

After condensation, the liquid refrigerant is subcooled in the GHX before evaporating at low temperature in the evaporator, delivering the useful cooling capacity $\dot{Q}_{evap}$. The gas mixture leaving the evaporator passes successively through the compressor and the ejector, where its pressure and velocity are increased, thereby improving the system's overall COP. At the inlet of the ejector, the refrigerant vapour entrains the weak solution returning from the generator, accelerating it toward the absorber. The exothermic absorption of ammonia into the aqueous solution in the absorber releases heat $\dot{Q}_{abs}$ (Mazouz et al. 2014). The cycle then repeats.

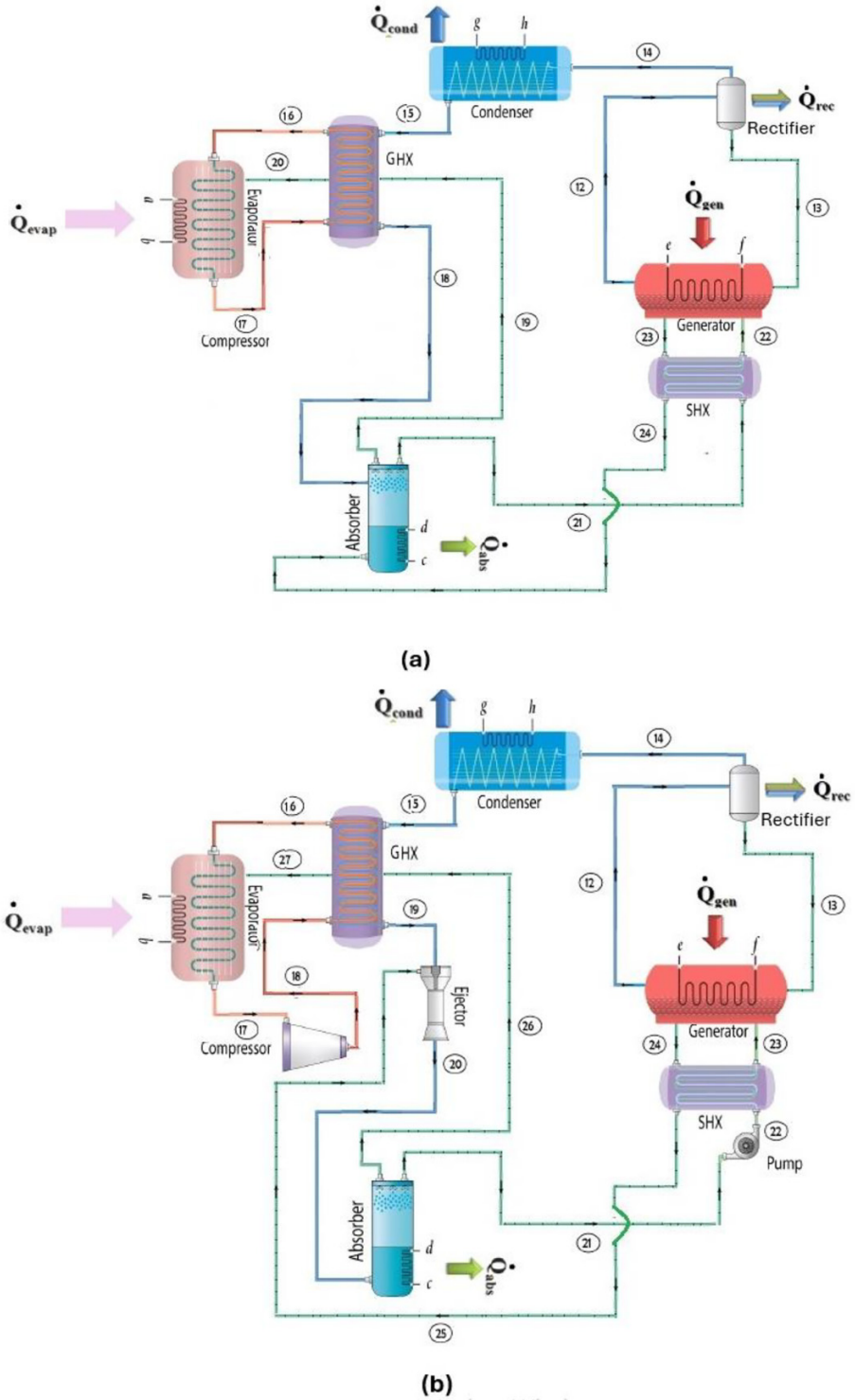
For clarity, Fig. 2*a* illustrates the conventional DAR cycle, while Fig. 2*b* presents the modified DAR-EC configuration. The main distinction between the two systems lies in the addition of the ejector and the compressor, which enable enhanced pressure management and improved performance.

2.2. Absorption working fluids selection

Selecting an appropriate working fluid is a critical step in the design and operation of any heat-recovery refrigeration system. The fluid's thermophysical properties strongly influence overall performance. Key factors include evaporation behaviour at saturation, safety considerations (especially in the event of leaks or accidental releases), and the substance's GWP. Because different fluids exhibit distinct evaporation characteristics, safety profiles, and environmental impacts, the choice of working fluid is central to determining system efficiency and reliability.

Thermodynamic properties are typically represented using property diagrams. According to Cefarin (2015), the most critical parameters for designing an absorption system include pressure, temperature, mass fraction, enthalpy, specific volume, and entropy. Among available working pairs, the water–ammonia mixture is widely used for its effectiveness in absorption refrigeration cycles and its ability to utilize low-grade heat sources in the 80–200 °C range. In the present study, a ternary water–ammonia–hydrogen mixture is employed. This selection is motivated by its favourable performance characteristics and its suitability for exploiting low-temperature heat sources.

Fig. 2. (*a*) Scheme of diffusion–absorption refrigeration cycle and (*b*) scheme of DAR-EC cycle. DAR-EC, diffusion–absorption refrigeration (DAR) system enhanced with an ejector and a compressor



3. Benefits, safety risks, and remedies of using ammonia

Ammonia is a flammable refrigerant with an auto-ignition temperature of approximately 651 °C and an octane number of 130 (Aziz et al. 2023), both higher than those of methane and propane. According to Shanmugam and Mital (2019), anhydrous ammonia is widely used in large-scale refrigeration systems due to its superior thermodynamic properties, offering 3%–10% higher efficiency compared with competing refrigerants. Ammonia also has an ozone-depletion potential and a GWP of zero (Mehr et al. 2013; Han et al. 2014; Shanmugam and Mital 2019; Yamamoto et al. 2022). As noted by Yamamoto et al. (2022), the water–ammonia pair is

Trans. Can. Soc. Mech. Eng. Downloaded from cdnsciencepub.com by Ecole de technologie superieure on 09/25/26

Trans. Can. Soc. Mech. Eng. Downloaded from cdnsciencepub.com by Ecole de technologie superieure on 09/25/26

Table 2. Operating parameters of the DAR and DAR-EC systems.

Operating parameters	Values
Gas temperature at generator inlet ($T_{gas\text{-}gen}$)	109.5 °C
The mass flow rate of working fluid ($H_2O + NH_3$)	22.32 kg/s
The mass flow rate of H_2	14.83 kg/s
Ambient temperature	30°C
Rectifier pinch-point temperature difference	10°C
The efficiency of the absorber	80% (Long et al. 2013)
The efficiency of the evaporator	80%
The efficiency of heat exchangers	70% (Hu et al. 2023)
The concentration of NH_3 in the mixture at the pump discharge	30% (Yousuf et al. 2014)
Evaporator pinch-point temperature difference	10°C (Mansouri et al. 2017)
SHX efficiency	70% (Hu et al. 2023)
Efficiency of the diffuser (ejector)	85% (Khan et al. 2025, 2023)
Efficiency of the nozzle (ejector)	85% (Khan et al. 2025, 2023)
Efficiency of mixer (ejector)	95% (Khan et al. 2025, 2023)
Efficiency of the compressor	85% (Khan et al. 2025, 2023)

Note: DAR, diffusion–absorption refrigeration; DAR-EC, diffusion–absorption refrigeration system enhanced with an ejector and a compressor; SHX, solution heat exchanger.

considered one of the most effective natural working fluids for absorption refrigeration systems and can operate over a wide temperature range. Because of these advantages, ammonia is recognized as a natural refrigerant that decomposes readily in the environment.

Despite its thermodynamic and environmental benefits, ammonia poses significant safety risks. At high concentrations (15%–28% by volume in air), it can cause severe skin and eye burns, respiratory damage, or even be fatal. Ammonia can also explode if released into an enclosed space in the presence of an ignition source, or if containers are exposed to sufficiently high temperatures (SCFP 2019; Shanmugam and Mital 2019). These hazards underscore the importance of rigorous leak prevention, proper ventilation, and regular inspection of pipes and storage vessels to ensure safe operation. In the United States, industrial ammonia refrigeration systems containing 4536 kg (10 lbs) or more are subject to OSHA's process safety management standard and the EPA's risk management program requirements (Shanmugam and Mital 2019).

4. Pressure and concentration limitations of the installation

Pressure is an essential parameter in the study of diffusion absorption refrigeration machines. It is also the main parameter (pressure level) used to classify absorption refrigeration machines (see Table 1). The safety of the installation and people is often cited as an argument for limiting pressure, since the working fluid is considered toxic and flammable. Eliminating leakage problems is a priority for this type of installation. Pressure limitation also has an economic advantage: it reduces the need for heavy safety devices, such as complex valves, etc.

In this article, hydrogen is used as an inert gas to lower the partial pressure of ammonia at the evaporator, as excessive pressure can affect the evaporator's efficiency. In the case of DAR-EC, the pressure level is very high due to the presence of the compressor and circulation pump, which can increase mechanical stress, reduce the service life of the seals and accessories in the circuit, and, above all, increase the cost of servicing and maintenance (which is virtually non-existent in the case of DAR). In terms of concentration, it is advisable to work at an optimal level; too high a concentration of NH_3 increases the risk of leaks and makes absorption in the absorber more difficult. Too low a concentration can reduce cooling power and absorption capacity.

5. Modeling of DAR and DAR-EC cycles

The following section presents the mathematical modelling approach used to describe the behaviour of the DAR and DAR-EC systems. The modelling procedure begins with the formulation of the main assumptions, followed by the development of mass, energy, and exergy balance equations for each cycle component. Finally, the mixing model used for the working fluids is introduced.

The overall analysis relies on the M2EP framework, which integrates mass conservation, energy conservation, exergy assessment, and performance (M2EP) evaluation. The modelling and optimization of the system are carried out using the PSO algorithm, enabling the identification of operating conditions that improve the system's COP.

5.1. Data of the study

The data and operating conditions required to simulate the multigeneration system are derived from an existing cement kiln located in Congo-Kinshasa. These technical and industrial inputs enable the realistic modelling of the proposed configuration. The operating parameters of the Kalina cycle used in this study are documented in Yousuf et al. (2014), while the principal parameters for the DAR and DAR-EC cycles are summarized in Table 2.

Table 3. Mass, energy, and exergy balance of diffusion–absorption refrigeration system.

Components	Mass balance equations	Energy balance equations	Exergy balance equations
Bubble pump	$\dot{m}_{22}+\dot{m}_{13}=\dot{m}_{12}+\dot{m}_{23}$	$\dot{Q}_{gen}=\dot{m}_{22}h_{22}+\dot{m}_{13}h_{13}-\dot{m}_{12}h_{12}-\dot{m}_{23}h_{23}$	$\dot{E}x_{13}+\dot{E}x_{22}=\dot{E}x_{12}+\dot{E}x_{23}+\dot{E}x^{D}_{gen}$
Rectifier	$\dot{m}_{12}=\dot{m}_{13}+\dot{m}_{14}$	$\dot{Q}_{rec}=\dot{m}_{12}h_{12}-\dot{m}_{13}h_{13}-\dot{m}_{14}h_{14}$	$\dot{E}x_{14}+\dot{E}x_{13}=\dot{E}x_{12}+\dot{E}x^{D}_{rec}$
Condenser	$\dot{m}_{14}=\dot{m}_{15}$	$\dot{Q}_{cond}=\dot{m}_{14}(h_{15}-h_{14})$	$\dot{E}x_{15}=\dot{E}x_{14}+\dot{E}x^{D}_{Cond}$
GHX exchanger	$\dot{m}_{15}=\dot{m}_{16}$ $\dot{m}_{17}=\dot{m}_{18}$ $\dot{m}_{19}=\dot{m}_{20}$	$\dot{Q}_{GHX}=\dot{m}_{15}(h_{16}-h_{15})=\dot{m}_{17}(h_{18}-h_{17})=\dot{m}_{19}(h_{20}-h_{19})$	$\dot{E}x_{15}+\dot{E}x_{17}+\dot{E}x_{19}=\dot{E}x_{16}+\dot{E}x_{18}+\dot{E}x_{20}+\dot{E}x^{D}_{GHX}$
Evaporator	$\dot{m}_{16}+\dot{m}_{20}=\dot{m}_{17}$	$\dot{Q}_{evap}=\dot{m}_{17}h_{17}-\dot{m}_{16}h_{16}-\dot{m}_{20}h_{20}$	$\dot{E}x_{16}+\dot{E}x_{20}=\dot{E}x_{17}+\dot{E}x^{D}_{evap}$
Absorber	$\dot{m}_{18}+\dot{m}_{24}=\dot{m}_{19}+\dot{m}_{21}$	$\dot{Q}_{abs}=\dot{m}_{18}h_{18}+\dot{m}_{24}h_{24}-\dot{m}_{19}h_{19}-\dot{m}_{21}h_{21}$	$\dot{E}x_{24}+\dot{E}x_{18}=\dot{E}x_{21}+\dot{E}x_{19}+\dot{E}x^{D}_{abs}$
SHX exchanger	$\dot{m}_{21}=\dot{m}_{22}$ AND $\dot{m}_{23}=\dot{m}_{24}$	$\dot{Q}_{SHX}=\dot{m}_{21}(h_{22}-h_{21})=\dot{m}_{23}(h_{24}-h_{23})$	$\dot{E}x_{23}+\dot{E}x_{21}=\dot{E}x_{24}+\dot{E}x_{22}+\dot{E}x^{D}_{SHX}$

Note: GHX, gas heat exchanger; SHX, solution heat exchanger.

Table 4. Mass, energy, and exergy balance of DAR-EC (diffusion–absorption refrigeration system enhanced with an ejector and a compressor) system.

Components	Mass balance equations	Energy balance equations	Exergy balance equations
DAR-EC system			
Bubble pump	$\dot{m}_{22}+\dot{m}_{13}=\dot{m}_{12}+\dot{m}_{23}$	$\dot{Q}_{gen}=\dot{m}_{22}h_{22}+\dot{m}_{13}h_{13}-\dot{m}_{12}h_{12}-\dot{m}_{23}h_{23}$	$\dot{E}x_{13}+\dot{E}x_{22}=\dot{E}x_{12}+\dot{E}x_{23}+\dot{E}x^{D}_{gen}$
Rectifier	$\dot{m}_{12}=\dot{m}_{13}+\dot{m}_{14}$	$\dot{Q}_{rec}=\dot{m}_{12}h_{12}-\dot{m}_{13}h_{13}-\dot{m}_{14}h_{14}$	$\dot{E}x_{14}+\dot{E}x_{13}=\dot{E}x_{12}+\dot{E}x^{D}_{rec}$
Condenser	$\dot{m}_{14}=\dot{m}_{15}$	$\dot{Q}_{cond}=\dot{m}_{14}(h_{15}-h_{14})$	$\dot{E}x_{15}=\dot{E}x_{14}+\dot{E}x^{D}_{Cond}$
GHX exchanger	$\dot{m}_{15}=\dot{m}_{16}$ $\dot{m}_{18}=\dot{m}_{19}$ $\dot{m}_{26}=\dot{m}_{27}$	$\dot{Q}_{GHX}=\dot{m}_{15}(h_{16}-h_{15})=\dot{m}_{18}(h_{19}-h_{18})=\dot{m}_{26}(h_{27}-h_{26})$	$\dot{E}x_{15}+\dot{E}x_{18}+\dot{E}x_{26}=\dot{E}x_{16}+\dot{E}x_{19}+\dot{E}x_{27}+\dot{E}x^{D}_{GHX}$
Evaporator	$\dot{m}_{16}+\dot{m}_{27}=\dot{m}_{17}$	$\dot{Q}_{evap}=\dot{m}_{17}h_{17}-\dot{m}_{16}h_{16}-\dot{m}_{27}h_{27}$	$\dot{E}x_{16}+\dot{E}x_{27}=\dot{E}x_{17}+\dot{E}x^{D}_{evap}$
Compressor	$\dot{m}_{17}=\dot{m}_{18}$	$\dot{W}_{Comp}=\dot{m}_{17}(h_{18}-h_{17})$	$\dot{E}x_{18}=\dot{E}x_{17}+\dot{E}x^{D}_{Comp}$
Ejector	$\dot{m}_{19}+\dot{m}_{25}=\dot{m}_{20}$	$\dot{Q}_{Eject}=\dot{m}_{19}h_{19}+\dot{m}_{25}h_{25}-\dot{m}_{20}h_{20}$	$\dot{E}x_{19}+\dot{E}x_{25}=\dot{E}x_{20}+\dot{E}x^{D}_{Eject}$
Absorber	$\dot{m}_{20}=\dot{m}_{26}+\dot{m}_{21}$	$\dot{Q}_{abs}=\dot{m}_{20}h_{20}-\dot{m}_{26}h_{26}-\dot{m}_{21}h_{21}$	$\dot{E}x_{20}=\dot{E}x_{26}+\dot{E}x_{21}+\dot{E}x^{D}_{abs}$
SHX exchanger	$\dot{m}_{22}+\dot{m}_{24}=\dot{m}_{23}+\dot{m}_{25}$	$\dot{Q}_{SHX}=\dot{m}_{22}h_{22}+\dot{m}_{24}h_{24}-\dot{m}_{23}h_{23}-\dot{m}_{25}h_{25}$	$\dot{E}x_{22}+\dot{E}x_{24}=\dot{E}x_{23}+\dot{E}x_{25}+\dot{E}x^{D}_{SHX}$
Pump	$\dot{m}_{21}=\dot{m}_{22}$	$\dot{W}_{Pump}=\dot{m}_{21}(h_{22}-h_{21})$	$\dot{E}x_{22}=\dot{E}x_{21}+\dot{E}x^{D}_{Pump}$

Note: GHX, gas heat exchanger; SHX, solution heat exchanger.

5.2. M2EP (mass, energy, exergy, and performance) analysis method

In the literature, several analysis methodologies have been proposed to evaluate the performance of energy systems. According to Mofrad et al. (2023) and Fazeli et al. (2022), modern technologies increasingly prioritize energy efficiency, cost-effectiveness, and environmental performance from the design stage onward. Consequently, energy, exergy, exergoeconomic, and exergoenvironmental (4E) analyses are widely employed to investigate and understand the behaviour of industrial systems. Kayes et al. (2024) further demonstrated the relevance of this approach by applying the 4E methodology to the analysis of a triple-cascade refrigeration system. In this work, the thermodynamic modelling of both the DAR and DAR-EC systems is carried out using the M2EP analysis framework, which combines mass, energy, and exergy balances with overall performance evaluation. This integrated approach enables a comprehensive assessment of both individual cycle components and the system as a whole.

Tables 3, 4, and 5 present the mass, energy, and exergy balance equations governing the individual components of the DAR and DAR-EC configurations. These equations are formulated in accordance with the first and second laws of thermodynamics. In addition, the performance indicators, including the COP, cooling capacity, compressor work, pump work, and isentropic efficiency, are defined for both systems. Together, these equations and performance parameters form the basis of the thermodynamic and exergetic analysis used in this study.

Table 6 provides a clearer understanding of the various numerical indices used in the equations in Tables 3–5. These indices represent the points in the cycles shown in Fig. 2.

Based on the literature (Liu et al. 2023; Kumar and Modi 2024; Khan et al. 2024*b*), the mass balance is formulated using

Trans. Can. Soc. Mech. Eng. Downloaded from cdnsciencepub.com by Ecole de technologie superieure on 09/25/26

Trans. Can. Soc. Mech. Eng. Downloaded from cdnsciencepub.com by Ecole de technologie superieure on 09/25/26

Table 5. Performance parameters of DAR and DAR-EC systems.

Components	Performance parameters
DAR system	
COP	$COP = \frac{\dot{Q}_{evap}}{\dot{Q}_{gen}}$
Temperature of evaporator	$T_{evap} = (1 - \varepsilon)\, T_{amb} + \varepsilon T_{16}{}^{*}$
Net cooling capacity	$\dot{Q}_{evap} = \dot{m}_{17}h_{17} - \dot{m}_{16}h_{16} - \dot{m}_{20}h_{20}$
DAR-EC system	
COP	$COP = \frac{\dot{Q}_{evap}}{\dot{Q}_{gen}+\dot{W}_{comp}+\dot{W}_{pump}}$
Net cooling capacity	$\dot{Q}_{evap} = \dot{m}_{17}h_{17} - \dot{m}_{16}h_{16} - \dot{m}_{27}h_{27}$
Net power of the compressor	$\dot{W}_{comp} = \dot{m}_{17}\frac{h_{18s}-h_{17}}{\eta_{s\,comp}}$
Net power of the pump	$\dot{W}_{pump} = \dot{m}_{21}\frac{h_{22s}-h_{21}}{\eta_{s\,pump}}$
Isentropic efficiency of the compressor	$\eta_{Scomp} = \frac{h_{18}-h_{17}}{h_{18s}-h_{17}}$

Note: DAR, diffusion–absorption refrigeration; DAR-EC, diffusion–absorption refrigeration system enhanced with an ejector and a compressor; COP, coefficient of performance.

*Formula established based on the following relationship: $\varepsilon_{vap} = \frac{T_{amb}-T_{evap}}{T_{amb}-T_{16}}$, h_{18s} is the isentropic outlet enthalpy of the compressor.

Table 6. Cycle points and their meaning.

DAR		DAR-EC	
Cycle points	Meaning/interpretation	Cycle points	Meaning/interpretation
12	Generator output and rectifier input	12	Generator output and rectifier input
13	Rectifier output and generator input	13	Rectifier output and generator input
14	Rectifier output and condenser input	14	Rectifier output and condenser input
15	Condenser output and GHX input	15	Condenser output and GHX input
16	GHX output and evaporator input	16	GHX output and evaporator input
17	Evaporator output and GHX input	17	Evaporator outlet and compressor inlet
18	GHX outlet and absorber inlet	18	Compressor outlet and GHX inlet
19	Absorber outlet and GHX inlet	19	GHX outlet and ejector inlet
20	GHX outlet and evaporator inlet	20	Ejector outlet and absorber inlet
21	Absorber outlet and SHX inlet	21	Absorber outlet and pump inlet
22	SHX outlet and generator inlet	22	Pump outlet and SHX inlet
23	Generator outlet and SHX inlet	23	SHX output and generator input
24	SHX outlet and absorber inlet	24	Generator output and SHX input
–	–	25	SHX output and ejector input
–	–	26	Absorber output and GHX input
–	–	27	GHX output and evaporator input

Note: DAR, diffusion–absorption refrigeration; DAR-EC, diffusion–absorption refrigeration system enhanced with an ejector and a compressor; SHX, solution heat exchanger; GHX, gas heat exchanger.

the mass flow rate $\dot{m}_i$, where subscript i denotes the different thermodynamic states (points) of the cycle. For each system component operating under steady-state conditions, the sum of the inlet mass flow rates is equal to the sum of the outlet mass flow rates (Zhang et al. 2023*a*):

$$\sum_{i}^{inlet} \dot{m}_i = \sum_{i}^{outlet} \dot{m}_i$$

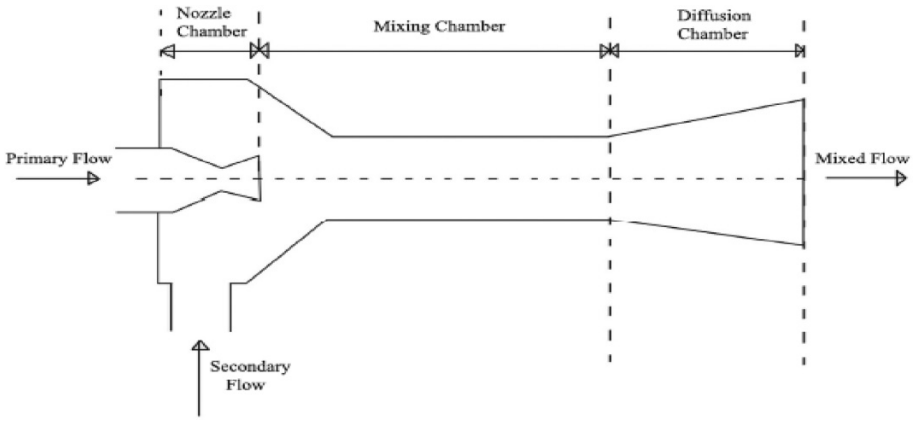
Energy exchanges within the system are expressed in terms of heat transfer rates $\dot{Q}j$ and work rates $\dot{W}_j$, where j represents the system components that supply or consume heat and work. The energy balance for each component is formulated as a function of the mass flow rates and the specific enthalpies of the corresponding cycle states, such that:

$$\dot{Q}_j - \dot{W}_j = \sum_{i}^{outlet} \dot{m}_i h_i - \sum_{i}^{inlet} \dot{m}_i h_i$$

where h_i is the specific enthalpy of each state (specific enthalpy point) of the cycle (Liu et al. 2023; Khan et al. 2024*b*).

According to Zhang et al. (2023*a*), the exergy balance is expressed by equating the sum of the incoming exergy rates to the sum of the outgoing exergy rates plus the exergy

Fig. 3. Schematic diagram of the ejector. Reprinted from Khan et al. (2025) with permission from Elsevier.



destruction associated with the component:

$$\sum_{i}^{\text{inlet}} \dot{E}\, x_i = \sum_{i}^{\text{outlet}} \dot{E}\, x_i + \dot{E}\, x_j^D$$

where $\dot{E}\, x_j^D$ represents the exergy destruction due to irreversibilities within component j. Regarding performance indicators, the COP of the DAR cycle is modelled following the approach presented in Zhang et al. (2023*b*). For the DAR-EC configuration, the COP formulation is based on the methodology proposed by Kumar and Modi (2024). The compressor and pump power consumptions are calculated using their respective isentropic efficiencies, as described in Khan et al. (2024*b*).

5.3. Application of the particle swarm optimization (PSO) algorithm

Given that the performance evaluation of the DAR and DAR-EC cycles requires varying several operating parameters and incorporating additional components governed by nonlinear equations (such as the ejector), solving for specific variables, particularly temperatures, pressures, and NH_3 concentrations, becomes complex. For this reason, the PSO technique was adopted to facilitate parameter optimization.

According to Pu et al. (2026), PSO is an adaptive search algorithm that dynamically adjusts the optimisation process based on real-time feedback from the system under study, thereby overcoming the limitations of static optimisation parameters. In situations where input or operating parameters must be modified, PSO is frequently employed to prevent solution degradation and reduce significant numerical errors, enabling more accurate optimisation and correction of inaccuracies introduced by parameter-adjustment methods (An et al. 2025). Cheng et al. (2025) demonstrated the effectiveness of an improved PSO approach, incorporating neighbourhood diversity learning, in addressing reduced planning accuracy in multi-energy coupling within integrated regional energy systems.

In the present work, PSO is combined with the M2EP framework (see Section 5.2) to identify the maximum cooling capacity and the optimal COP for both the DAR and DAR-EC cycles. The algorithm is explicitly applied to maximise key performance indicators, with a focus on enhancing COP across the studied operating conditions.

5.4. Main assumptions

In this study, the following assumptions are adopted for the modelling of both the DAR and DAR-EC cycles:

- Temperature variations directly affect the ammonia (NH_3) concentration in the working mixture.
- The temperatures at points 24 and 15 are equal ($T_{24} = T_{15}$).
- At the inlet, the working fluid composition is fixed at 88% NH_3 and 12% H_2O by mass.
- The entire process operates under steady-state conditions.

Additional assumptions and fixed operating parameters are provided in Table 2. Assumptions were used to reduce the complexity of the model. Future work should focus on gradually reducing the assumptions to refine the results of the present model.

5.5. Equations governing the ejector

The ejector in the absorption cycle is modelled as a simple, one-dimensional device. It is assumed that the velocities of both the primary and secondary refrigerant streams are uniform along the ejector and across all internal cross-sections. This common simplifying assumption is supported by several studies (Chen et al. 2013; Majdi 2016; Al-Hamed and Dincer 2019; Khalili and Garousi Farshi 2020; Sanaye and Refahi 2020).

Figure 3 illustrates the main components of the ejector: the nozzle, mixing chamber, and diffuser. The characteristic equations describing mass, momentum, and energy conservation in each region are summarized in Table 7. These relations are used to determine the pressure, velocity, and mixing conditions of the flow through the ejector and, ultimately, to evaluate its influence on the overall performance of the DAR-EC cycle.

Since the ejector in absorption–diffusion refrigeration machines (MFAD) operates in a steady state, it can be modelled

Trans. Can. Soc. Mech. Eng. Downloaded from cdnsciencepub.com by Ecole de technologie superieure on 09/25/26

Table 7. Equations of the ejector.

Nozzle section	$h_{pf,2} + \frac{u_{pf,2}^2}{2} = h_{pf,1} + \frac{u_{pf,1}^2}{2}$
Mixing section	$\dot{m}_{pf}u_{pf,n2} + \dot{m}_{sf}u_{sf,n2} = \left(\dot{m}_{pf} + \dot{m}_{sf}\right) h_{mf,m,id} \dot{m}_{pf}\left(h_{pf,2} + \frac{u_{pf,2}^2}{2}\right) + \dot{m}_{sf}\left(h_{sf,2} + \frac{u_{sf,2}^2}{2}\right) = \left(\dot{m}_{pf} + \dot{m}_{sf}\right)\left(h_{mf,m} + \frac{u_{mf,m}^2}{2}\right)$
Diffuser section	$h_{mf,d,s} - h_{mf,m} = \frac{u_{mf,m}^2 - u_{mf,d,s}^2}{2} h_{mf,d} - h_{mf,m} = \frac{u_{mf,m}^2 - u_{mf,d}^2}{2}$
Back pressure	$p_b = p_{\text{suction}} - \Delta p$

using a one-dimensional (1D) model based on the ternary mixture $NH_3/H_2O/H_2$. This model describes the dominant mechanisms of momentum transfer between the ammonia-rich primary jet and the secondary fluid, while maintaining a level of computational complexity compatible with integration into a system model.

The 1D model is particularly suitable for predicting overall system performance, such as entrainment rate, outlet pressures, and mass flow rates. In the literature (Dhahi Gharir and Farshi 2023; Khan et al. 2025; Siddique et al. 2025), for compressible flows with axisymmetric geometry, thermodynamic, and kinematic quantities are often treated as averages over the characteristic sections of the ejector (nozzle, mixing, and diffuser). This approach is justified when the objective is to evaluate overall performance, as is the case in this work.

6. Results and discussions

6.1. Thermodynamic performance

6.1.1. DAR cycle

The thermodynamic performance of the DAR cycle is assessed using the first and second laws of thermodynamics, which describe the conservation of energy and the degradation of energy quality, respectively. Energy analysis involves quantifying the heat supplied to and rejected by each component, while the exergy balance provides insight into irreversibilities and the sources of performance losses within the system. In this study, the performance evaluation focuses on the COP, evaporation temperature, cooling capacity, and the distribution of heat and exergy flows among the cycle's main components.

Using the available heat flux of 7368 kW at 109.5 °C from the Kalina cycle (see Table 2), the distribution of heat exchanges within the DAR system is presented in Fig. 4. The absorber accounts for the largest share of heat rejection (≈36%), followed by the generator (≈35%). The remaining heat is distributed among the condenser, rectifier, and evaporator, each contributing a smaller fraction to the total heat exchange.

The dominant heat rejection in the absorber is attributed to the mass transfer between the refrigerant vapour and the diluted solution. This absorption process occurs under significant concentration gradients, leading to substantial heat release. Similarly, the high heat input at the generator results from the large temperature difference between the hot exhaust gases and the water–ammonia solution, combined with ammonia's favourable thermophysical properties, particularly its high latent heat of vaporization. In addition, the volatility difference between ammonia and water promotes effective separation within the generator, further contributing to the observed heat exchange.

Fig. 4. Distribution of heat exchanges of the diffusion–absorption refrigeration cycle.

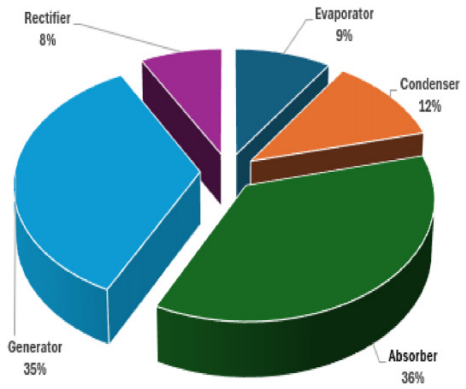
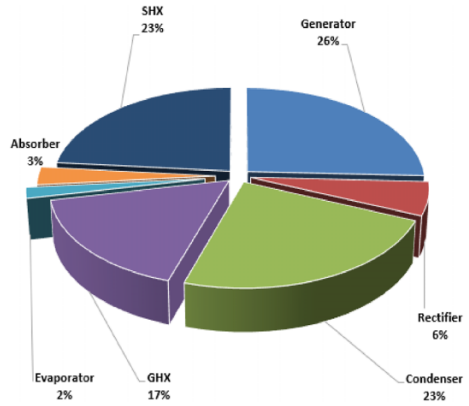


Fig. 5. Distribution of exergy destroyed in the different components of the diffusion–absorption refrigeration.



The rectifier exhibits a relatively low heat exchange rate (approximately 8%), indicating efficient operation. This behaviour is expected, as the rectifier primarily functions as a purification component rather than a major heat exchanger. The small heat-transfer surface area explains the limited heat transfer, the low temperature gradient, and the comparatively low turbulence level within the rectification zone.

Figure 5 illustrates the distribution of exergy destruction among the DAR system components. The generator exhibits the highest exergy destruction, accounting for approximately

Trans. Can. Soc. Mech. Eng. Downloaded from cdnsciencepub.com by Ecole de technologie superieure on 09/25/26

Trans. Can. Soc. Mech. Eng. Downloaded from cdnsciencepub.com by Ecole de technologie superieure on 09/25/26

26% of the total, followed by the condenser (23%), the solution heat exchanger (SHX), and the gas heat exchanger (GHX). In contrast, the evaporator contributes only about 2% of the total exergy losses.

The high exergy destruction observed in the generator is expected, as it is the primary component of both the DAR and DAR-EC configurations. This behaviour results from several factors: the input of high-exergy thermal energy from cement-kiln exhaust gases, the large temperature difference between the hot gases and the water–ammonia solution, and the irreversible separation processes occurring within the generator. These effects are further intensified by high concentration gradients and strong thermal gradients, which collectively increase entropy generation.

Similarly, the condenser exhibits substantial exergy destruction due to diffusion and thermal resistance phenomena, as well as the absence of a heat-recovery mechanism. A significant fraction of the available exergy is therefore discharged to the environment, with heat transfer occurring under finite temperature differences. The GHX and SHX also contribute to exergy destruction, which is attributed to the coexistence of temperature and concentration gradients within these exchangers, thereby limiting their exergetic efficiency.

By contrast, the evaporator displays a relatively low exergy destruction rate. This is primarily because it operates with nearly pure ammonia and does not involve mixture separation or chemical interactions, unlike the generator and absorber. The phase change in the evaporator occurs under quasi-isothermal conditions, resulting in low entropy production and reduced dissipative effects. Since lower exergy destruction is generally associated with improved system performance, these results emphasize the generator's dominant role and the importance of minimizing irreversibilities in this component.

6.1.2. DAR-EC cycle

The thermodynamic analysis of the DAR-EC cycle follows the same principles applied to the DAR system, combining energy and exergy assessments governed by the first and second laws of thermodynamics. The key difference lies in the addition of a compressor upstream of the ejector, which increases the refrigerant pressure before mixing. Together, the compressor and ejector enhance the driving potential for mass transfer in the absorber, thereby improving overall performance compared with the basic DAR cycle.

Figure 6 shows the distribution of heat exchanges among the DAR-EC components. As in the conventional DAR cycle, the absorber rejects the largest share of heat (36%), followed by the generator (31%). The evaporator accounts for a larger heat contribution (16%) than in the DAR configuration, while the remainder is divided between the condenser and the rectifier. The analysis in Subsection 6.1.1 on the heat exchange rates of cycle components also applies to DAR-EC.

The combined effect of the compressor and the ejector increases refrigerant circulation and improves thermodynamic conditions in the absorber and evaporator. These enhancements result in a higher cooling capacity and a significantly improved COP for the DAR-EC system relative to the conventional DAR cycle.

Fig. 6. Distribution of heat exchanges of diffusion–absorption refrigeration system enhanced with an ejector and a compressor cycle.

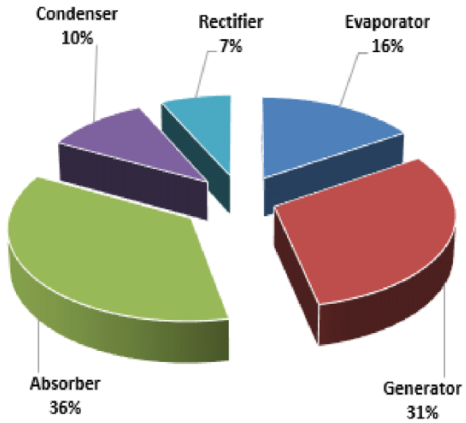


Table 8. Performance parameters.

Operating parameters	DAR	DAR-EC
Heat transfer rate from evaporator [kW]	6766	12 949
Heat transfer rate from condenser [kW]	8464	8428
Heat transfer rate from absorber [kW]	26 322	29 484
Heat transfer rate from generator [kW]	25 226	25 117
Heat transfer rate from rectifier [kW]	5743	5718
Coefficient of performance [–]	0.27	0.49

Note: DAR, diffusion–absorption refrigeration; DAR-EC, diffusion–absorption refrigeration system enhanced with an ejector and a compressor.

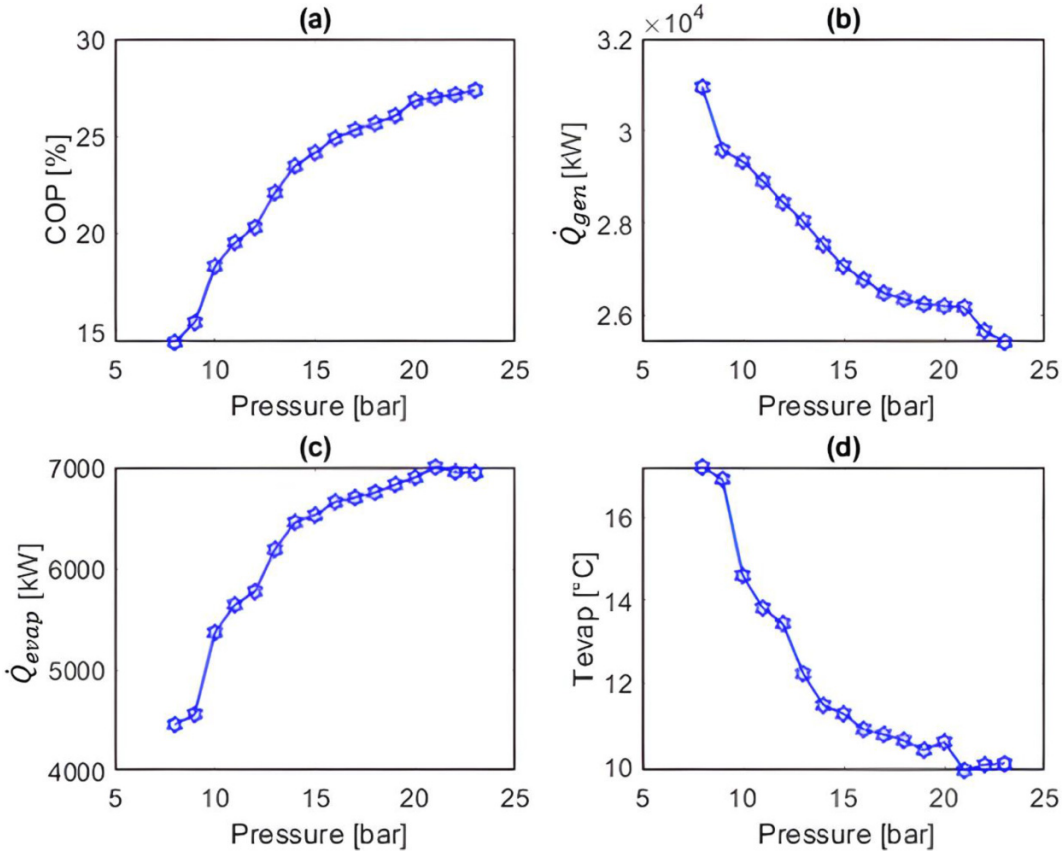
6.2. Comparison between DAR and DAR-EC

Table 8 presents a comparison of the key performance parameters for the DAR and DAR-EC cycles. The results show that integrating a compressor and an ejector significantly enhances system performance. In particular, the DAR-EC configuration exhibits a much higher heat transfer rate at the evaporator, nearly doubling that of the conventional DAR system. This improvement is directly linked to the increased refrigerant circulation and higher pressure levels achieved through compression and ejector entrainment.

The COP also increases substantially, rising from 0.27 for the DAR cycle to 0.49 for the DAR-EC system. This enhancement reflects the combined thermodynamic benefits of boosting absorber pressure, improving mass transfer, and increasing the driving potential for evaporation. Other heat-exchange components, such as the condenser, absorber, generator, and rectifier, show smaller relative variations between the two cycles, indicating that the main performance gains arise from the additional compression–ejector stage.

Overall, the DAR-EC configuration demonstrates markedly superior performance, particularly in cooling capacity and COP, confirming the effectiveness of integrating an ejector and a compressor into the diffusion–absorption cycle.

Fig. 7. Sensitivity to the cycle pressure variation of the (*a*) coefficient of performance (COP), (*b*) generator power, (*c*) evaporator power, and (*d*) temperature of the evaporator.



At the ejector inlet (point 19), the refrigerant pressure is significantly increased due to upstream compression. The pressure drop at the ejector outlet (point 20) plays a critical role in the performance of the DAR-EC system, as it is governed by the mixing process occurring in the mixing chamber between the lean solution (secondary flow originating from the generator through the SHX heat exchanger, point 25) and the NH_3-rich solution (primary or motive flow entering through the nozzle at point 19).

Although the secondary flow rate drawn through the suction nozzle is relatively small compared with the primary flow (see Fig. 3), its entrainment induces a pressure reduction at the ejector outlet according to $p_b = p_{\text{suction}} - \Delta p$ together with a slight increase in enthalpy at point 20. This mixing process enhances mass transfer in the absorber, leading to a significant increase in the absorber heat transfer rate $\dot{Q}_{\text{abs}}$, and, consequently, in the evaporator heat transfer rate $\dot{Q}_{\text{evap}}$. As a result, the cooling capacity increases by approximately 91%, rising from 6766 to 12 949 kW.

Since the generator heat input $\dot{Q}_{\text{gen}}$ remains nearly constant, the sum of $\dot{Q}_{\text{gen}}$, compressor work $\dot{W}_{\text{comp}}$ and pump work $\dot{W}_{\text{pump}}$ remains significantly lower than the enhanced evaporator load. This leads to a substantial increase in the coefficient of performance, defined as: -5

$$\text{COP} = \frac{\dot{Q}_{\text{evap}}}{\dot{Q}_{\text{gen}} + \dot{W}_{\text{comp}} + \dot{W}_{\text{pump}}}$$

To better quantify the contribution of the additional components, the overall COP improvement, from 0.27 to 0.49 (an increase of 0.22), was analysed. Simulation results indicate that the ejector is the dominant contributor to this improvement, accounting for 93.68% of the COP increase, while the compressor contributes the remaining 6.32%. In absolute terms, the ejector and compressor contribute 0.21 and 0.01, respectively, to the overall COP enhancement.

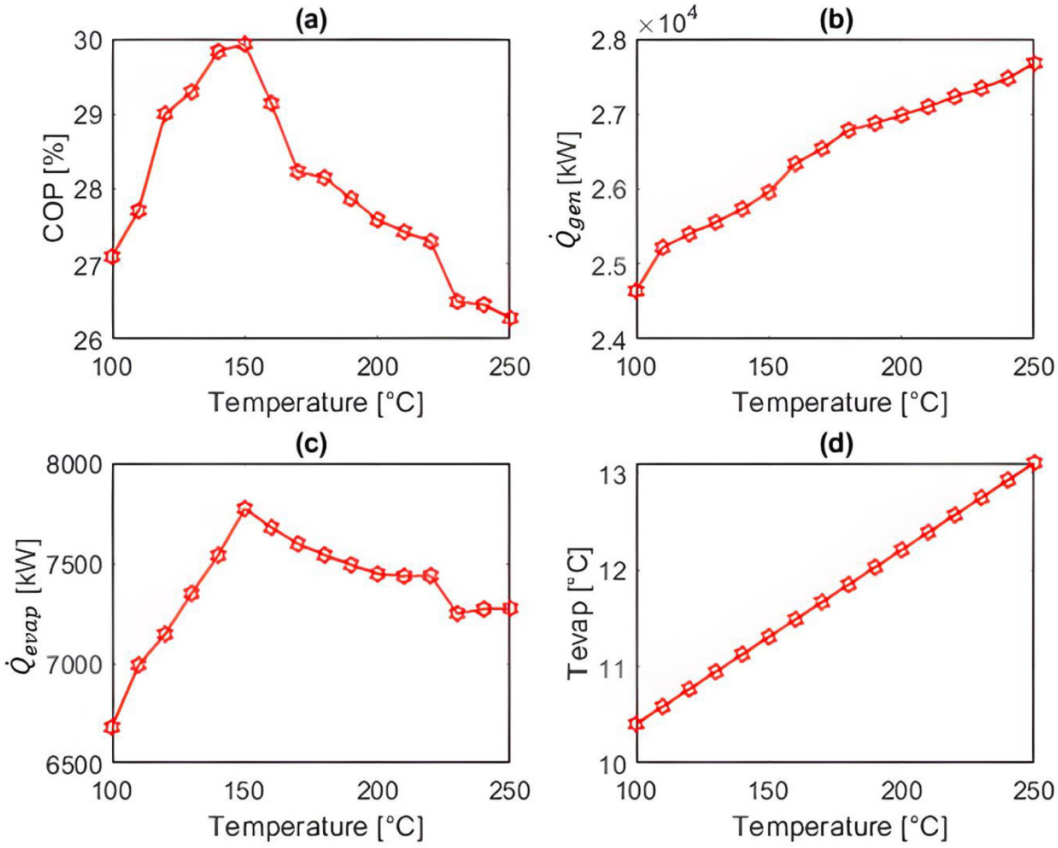
6.3. Sensitivity of the DAR System

The influence of pressure variation on the performance of the DAR cycle is illustrated in Fig. 7. As shown in Fig. 7*a*, the COP increases steadily with increasing system pressure, indicating improved thermodynamic conditions for the absorption–evaporation process. This behaviour is associated with enhanced ammonia desorption in the generator and an increase in the refrigerant mass flow rate. The rise in generator pressure, therefore, directly improves cooling.

In contrast, Fig. 7*b* shows that the generator heat input $\dot{Q}_{\text{gen}}$ decreases as pressure increases, reflecting reduced thermal requirements at higher operating pressures. This reduction

Trans. Can. Soc. Mech. Eng. Downloaded from cdnsciencepub.com by Ecole de technologie superieure on 09/25/26

Fig. 8. Influence of the generator's temperature variation on the (*a*) coefficient of performance (COP), (*b*) generator power, (*c*) evaporator power, and (*d*) temperature of the evaporator.



in generator heat transfer is governed by several factors, including improved ammonia desorption, enhanced internal heat recovery, reduced desorption heat demand, and a lower solution mass flow rate to be heated.

Figure 7*c* illustrates the effect of pressure on the evaporator heat transfer rate. The evaporator capacity increases proportionally with pressure, consistent with the higher refrigerant circulation rate through the cycle. This trend is also attributed to more intense evaporation in the evaporator and increased ammonia desorption in the generator.

Finally, Fig. 7*d* shows that the evaporation temperature decreases with increasing pressure, a characteristic of diffusion–absorption refrigeration systems operating at elevated pressures. An increase in generator pressure reduces the evaporation temperature because, for a given COP, each kilogram of NH_3 transports less energy. This effect is particularly pronounced at constant partial pressure, as the system adjusts to the NH_3–H_2O–H_2 equilibrium conditions in the evaporator.

Overall, these results confirm that system pressure is a key parameter governing DAR cycle performance, significantly influencing COP, generator heat input, evaporator capacity, and evaporation temperature.

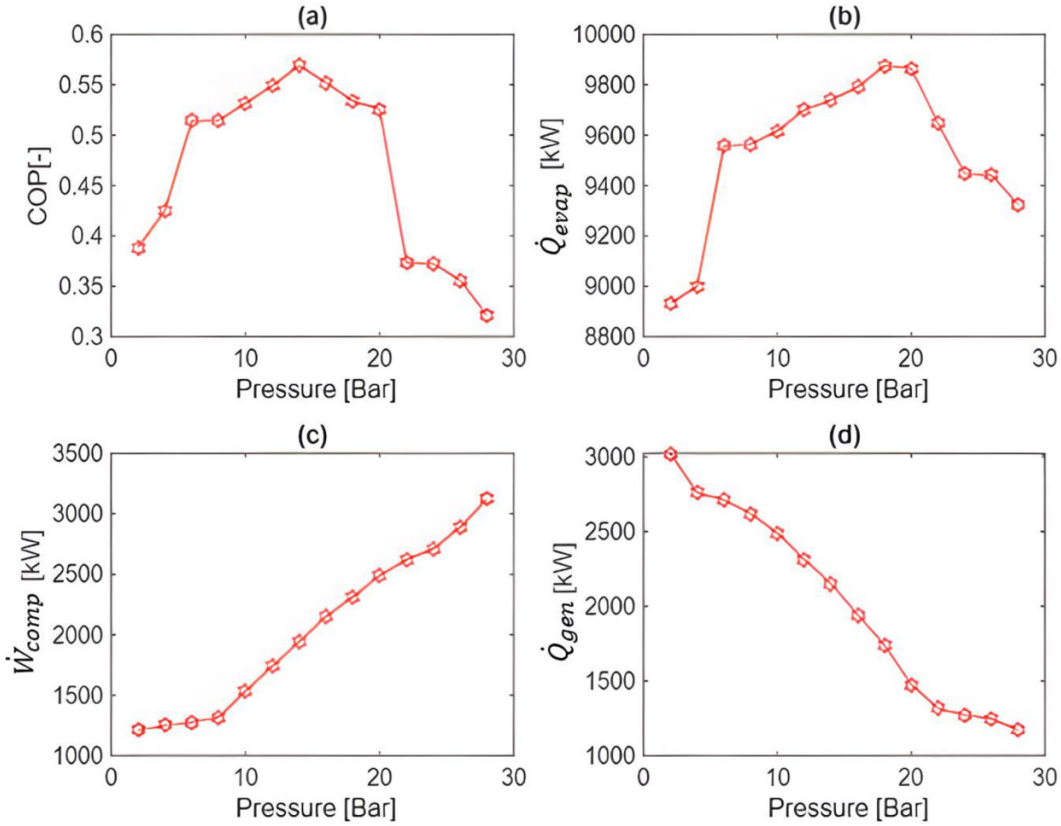
The influence of generator temperature variation on the performance of the DAR cycle is examined in Fig. 8. The discharge temperature of the Kalina cycle hot gases is used as the driving parameter, and the analysis is conducted over a temperature range of 100–250 °C, with increments of 10 °C.

Figure 8*a* shows the variation of the COP with generator temperature. The COP increases with temperature up to 150 °C, where it reaches a maximum value, and then decreases as the generator temperature rises further toward 250 °C. This behaviour indicates that high generator temperatures alone are not sufficient to ensure optimal system performance. Since the COP is directly related to the evaporator cooling capacity, a similar trend is observed for the evaporator heat transfer rate, as shown in Fig. 8*c*. Under constant pressure conditions, the evaporator power $\dot{Q}_{evap}$ increases with temperature until the optimal point, then decreases as the generator temperature continues to rise.

Figure 8*b* illustrates the variation of the generator heat input with generator temperature. The nonlinear shape of this curve is attributed to instabilities in the flow rates of both the hot exhaust gases and the water–ammonia solution. Finally, Fig. 8*d* shows a nearly linear increase in evaporator temperature with increasing generator temperature. Unlike the COP, the evaporator temperature continues to rise throughout the examined range, indicating a proportional relationship between generator and evaporator temperatures.

Trans. Can. Soc. Mech. Eng. Downloaded from cdnsciencepub.com by Ecole de technologie superieure on 09/25/26

Fig. 9. Effect of pressure variation on: (*a*) the coefficient of performance (COP), (*b*) the cooling capacity, (*c*) the power of the compressor, and (*d*) the power of the generator.



6.4. Sensitivity of the DAR-EC system

The influence of pressure variation on the performance of the DAR-EC cycle is illustrated in Fig. 9. The physical mechanisms discussed in Section 6.3 for the DAR system remain applicable to the DAR-EC configuration, with additional effects arising from the presence of the compressor.

As shown in Fig. 9*a*, the COP increases with pressure from 2 bar up to approximately 15 bar, where it reaches a maximum value of 0.556. Beyond this optimal point, the COP decreases as pressure continues to rise toward 28 bar, reflecting the increasing contribution of compressor work and the deterioration of thermodynamic conditions at higher pressure levels.

Figure 9*b* presents the corresponding variation of the cooling capacity Q_{evap}. At low pressures, the evaporator load increases gradually, then rises sharply once the pressure exceeds approximately 4.5 bar. The cooling capacity reaches a maximum at around 19 bar, after which it decreases with increasing pressure, indicating diminishing performance gains at higher pressures.

The compressor power requirement, shown in Fig. 9*c*, increases monotonically with pressure and reaches a maximum at 28 bar. This behaviour is expected due to the higher compression ratio imposed on the compressor at elevated system pressures. In addition, the increase in compressor heat transfer rate is associated with more effective NH_3 sorption and the higher refrigerant mass flow rate circulating through the system.

Finally, Fig. 9*d* shows that the generator heat input Q_{gen} decreases as pressure increases, exhibiting a trend similar to that observed for the conventional DAR cycle.

Overall, these results indicate that the DAR-EC cycle operates within an optimal pressure range in which both cooling capacity and COP are maximized. Operating beyond this range leads to excessive compressor work and a consequent reduction in overall system performance.

6.5. Sensitivity analysis of optimisation and robustness of the optimal solution

To better understand optimal operating conditions and assess the solution's robustness, a sensitivity analysis was conducted by varying two key parameters: generator pressure and generator temperature.

6.5.1. Influence of generator pressure

The sensitivity analysis for the DAR and DAR-EC systems, illustrated in Figs. 7 and 9, respectively, shows that increasing the generator pressure enables identification of an optimal operating point corresponding to a maximum COP.

For the DAR system, the COP reaches a maximum value of 0.27 at a generator pressure of $p_{gen} = 22.8$ bar. In contrast, the DAR-EC system exhibits an optimal COP of 0.57 at a lower generator pressure of $p_{gen} = 14.1$ bar. The evaporator heat transfer rate also reaches its maximum at specific pressure

Trans. Can. Soc. Mech. Eng. Downloaded from cdnsciencepub.com by Ecole de technologie superieure on 09/25/26

Trans. Can. Soc. Mech. Eng. Downloaded from cdnsciencepub.com by Ecole de technologie superieure on 09/25/26

levels: for the DAR system, a peak value of $\dot{Q}_{evap} = 7$ MW is observed at $p_{gen} = 22.8$ bar, while for the DAR-EC system, the maximum evaporator load $\dot{Q}_{evap} = 9.865$ MW occurs at $p_{gen} = 18.1$ bar.

Conversely, the generator heat transfer rate decreases as the generator pressure increases. For the DAR system, the minimum generator heat input of $\dot{Q}_{gen} = 25.50$ MW is obtained at $p_{gen} = 22.8$ bar. In the DAR-EC configuration, the minimum value of $\dot{Q}_{gen} = 1.22$ MW is reached at $p_{gen} = 28$ bar. These results indicate that the DAR-EC system is significantly more sensitive to variations in generator pressure than the conventional DAR system.

6.5.2. Influence of generator temperature

The sensitivity analysis with respect to generator temperature shows that increasing T_{gen} leads to the identification of an optimal operating point for both the COP and the evaporator heat transfer rate. This optimum is reached at a generator temperature of 150 °C, where the COP_{DAR} is 0.30, and the evaporator heat transfer rate is $\dot{Q}_{evap} = 7.75$ MW. Beyond this optimal temperature, the system's performance no longer improves, highlighting a temperature threshold above which additional heat input becomes less effective. In addition, both the evaporation temperature T_{evap} and the generator heat input $\dot{Q}_{gen}$ increase exponentially with increasing generator temperature, reflecting the system's strong dependence on this parameter.

6.5.3. Robustness of the optimal solution

The sensitivity analysis conducted near the optimal operating point shows that system performance remains stable under small variations in operating parameters. This behaviour indicates that the identified optimum is robust, with a sufficiently wide and acceptable operating range that tolerates continuous fluctuations in key system parameters without significant performance degradation.

6.6. Controllability and stability of the system to fluctuations in kiln exhaust gases

The controllability and operational stability of the two systems investigated in this study depend on their ability to manage thermal disturbances, particularly fluctuations in the flow rate and temperature of the kiln exhaust gases, to ensure reliable and efficient operation. In this context, the primary thermodynamic variables governing system control are the generator temperature and pressure, as well as the working fluid's internal mass flow rates, which respond to variations in the exhaust gas inlet conditions.

The sensitivity analysis presented in Subsection 6.4 reveals the existence of optimal operating points across relatively wide parameter ranges, thereby facilitating the controllability of both the DAR and DAR-EC systems. Among the key control parameters, the generator temperature (T_{gen}) offers a practical advantage over the generator pressure (p_{gen}), as it can be effectively regulated through exhaust gas flow control, bypass mechanisms, or the use of intermediate heat exchangers. As a result, the generator pressure behaves as a dependent variable, governed by the generator temperature according to $p_{gen} = f(T_{gen})$, making direct pressure regulation more challenging.

The thermal inertia of major components, such as the generator and the heat exchangers (GHX and SHX), helps maintain stable operation despite moderate fluctuations in furnace exhaust conditions. However, abrupt or large variations in exhaust gas temperature or flow rate may temporarily degrade system performance, leading to reductions in both the COP and the evaporator heat transfer rate.

7. Model validation

The validation of the proposed model is conducted in two stages: first for the DAR cycle and then for the DAR-EC configuration. In each case, the simulation results are compared with similar studies available in the literature, focusing on both operating conditions (inputs) and key performance indicators (outputs).

7.1. Comparison of DAR cycle system results with similar literature applications

To verify the accuracy of the DAR sub-model, the results obtained in this study are compared with those reported by Rattner and Garimella (2016*a*, 2016*b*). Table 9 presents the differences in input and output parameters between the two studies. Literature commonly uses ambient and generator temperatures of 24 and 130 °C, respectively. In contrast, the present model uses 30 °C for ambient air and 109 °C for the generator heat source. The working pressure in the literature is 11.5 bar, whereas the current simulation uses 20 bar, resulting in a difference of approximately 8.5 bar.

Despite these variations, the results for performance remain comparable. The reported COP in the literature is 0.260, while the present model predicts 0.268, a slight difference of 0.008. These similarities confirm that the DAR model developed in this work is consistent with previously validated studies and can be considered reliable.

7.2. Comparison of DAR-EC cycle system results with similar literature applications

The DAR-EC sub-model is validated by comparing its results with those reported by Khan et al. (2023). As in the DAR system validation, both operating conditions and performance indicators are examined. The main difference between the two studies lies in the generator temperature, which is 75 °C in the reference work and 109 °C in the present study. Other operating parameters are comparable, and the results summarized in Table 10 indicate that both models predict similar overall system behaviour.

The coefficient of performance reported by Khan et al. (2023) is 0.396, whereas the present model yields 0.490, a difference of 0.094. Differences in system configuration and modelling assumptions can explain this discrepancy. In the cycle proposed by Khan et al. (2023), the ejector is positioned immediately downstream of the evaporator, and the flow exiting the ejector passes through a flash tank before a portion

Table 9. Comparison between the results of the diffusion–absorption refrigeration (DAR) cycle of this model and those found in the literature.

Parameters	Rattner and Garimella (2016*a*, 2016*b*)	Present model	Gap
Type of refrigeration machine	DAR	DAR	–
Ambient temperature	24 °C	30 °C	+6 °C
Exchange temperature at the generator	130 °C	109 °C	−21 °C
Pressure	11.5 bars	20 bars	+8.5 bars
Working fluids	NH_3–NaSCN–He	NH_3–H_2O–H_2	–
COP found	0.260	0.268	+0.008

Note: COP, coefficient of performance.

Table 10. Comparison between the results of the DAR-EC cycle of this model and those found in the literature.

Parameters	Khan et al. (2023)	Present model	Gap
Type of refrigeration machine	DAR-EC	DAR-EC	–
Ambient temperature	25 °C	30 °C	+5 °C
Exchange temperature at the generator	75 °C	109 °C	+34 °C
Heat transfer rate from the evaporator	10 kW	12.95 kW	2.95 kW
Working fluids	NH_3–H_2O	NH_3–H_2O–H_2	–
COP found	0.396	0.490	0.094

Note: DAR, diffusion–absorption refrigeration; DAR-EC, diffusion–absorption refrigeration system enhanced with an ejector and a compressor; COP, coefficient of performance.

is directed to the compressor. In contrast, in the present configuration, the compressor is located directly at the evaporator outlet to increase the pressure at the ejector inlet, which is positioned downstream of the compressor. These structural differences are also linked to the choice of working fluid: binary in Khan et al. (2023) and ternary in the present study.

In addition, the higher generator temperature used in the present model contributes significantly to the observed COP difference. Previous studies have demonstrated the strong influence of generator temperature on COP (Kumar and Modi 2024; Mungyeko Bisulandu et al. 2024), showing that COP generally increases with generator temperature within the range of 0–150 °C. As the generator temperature in the present work is substantially higher than that employed by Khan et al. (2023), the resulting increase in COP is consistent with improved thermodynamic conditions.

Overall, the close agreement in cooling capacity and other performance parameters confirms that the DAR-EC model behaves as expected and supports the validity of the proposed configuration.

Several studies in the literature have investigated the sensitivity of generator pressure on the performance of DAR and DAR-EC cycles, including effects on the coefficient of performance, thermal power, heat transfer rates, and operating temperatures (Mohtaram et al. 2023; Zarei et al. 2023; Khan et al. 2024*a*). These findings confirm that the present study has appropriately identified and analysed the key operating variables governing the performance of the two systems.

8. Conclusions and perspectives

This study examined the thermal performance and the mass, energy, and exergy behaviour of a DAR-EC and operating with an H_2O–NH_3–H_2 working mixture. The analysis was conducted in three stages: (i) evaluation of a conventional DAR cycle, (ii) analysis of the modified DAR-EC configuration, and (iii) comparison of the results for both systems.

For the conventional DAR cycle, the model predicts a COP of 0.27, an evaporation temperature of 10.6 °C, and a cooling capacity of 6766 kW. Sensitivity analyses with respect to generator temperature and pressure yielded physically consistent trends, confirming the model's robustness. The corresponding hot-water temperature obtained in this work falls within the typical range of 40–50 °C used in residential heating applications.

To improve system performance, a compressor and an ejector were integrated into the DAR configuration. These components, placed at the evaporator outlet and the absorber inlet, respectively, increased pressure at key points in the cycle (points 18 and 19) and influenced the operation of several components, including the SHX heat exchanger. Despite operating downstream of the Kalina cogeneration cycle, where only low-temperature heat is available, the DAR-EC system delivered markedly improved performance. The COP increased substantially to 0.49, demonstrating the effectiveness of the ejector–compressor enhancement.

The comparative analysis confirms that the DAR-EC configuration outperforms the conventional DAR cycle, particularly in terms of cooling capacity and overall efficiency. Validation against published data further supports the reliability of the developed models.

8.1. Economic outlook for industrial applicability

The industrial applicability of DAR systems depends on both technological feasibility and economic viability. In practice, manufacturers and plant operators typically seek investments with a payback period of about 15 years. The de-

Trans. Can. Soc. Mech. Eng. Downloaded from cdnsciencepub.com by Ecole de technologie superieure on 09/25/26

Table 11. Qualitative economic evaluation of DAR and DAR-EC systems.

Post	Qualitative assessment
CAPEX	
Generator/absorber	Moderate
Condenser/evaporator	Comparable to a conventional system
Working fluid (NH_3–H_2O–inert gas)	Low
Instrumentation and control	Simple
Thermal integration	Varies depending on the site
OPEX	
Primary energy consumption	Waste heat recovery
Auxiliary power consumption	Very low (pump, control system)
Energy cost sensitivity	Low sensitivity, as it is an internal and free source
Maintenance costs	DAR: Low (no moving parts)
DAR-EC: moderate (presence of compressor)	
Working fluid costs	Natural, stable and less bulky fluids
Reliability and availability	High (low risk of mechanical failure)
Overall operating cost	Low to medium (energy context)

Note: DAR-EC, diffusion–absorption refrigeration system enhanced with an ejector and a compressor; DAR, diffusion–absorption refrigeration; CAPEX, capital expenditures; OPEX, operating expenditures.

Trans. Can. Soc. Mech. Eng. Downloaded from cdnsciencepub.com by Ecole de technologie superieure on 09/25/26

ployment of DAR systems is therefore primarily governed by capital expenditures (CAPEX) and operating expenditures (OPEX).

DAR systems are generally integrated into existing industrial or energy infrastructures, where the primary objective is to enhance overall energy efficiency. Compared with conventional vapor-compression refrigeration systems, DAR systems offer several advantages, including the absence of moving mechanical parts (which significantly reduces maintenance requirements), the ability to operate partially or entirely on low-grade or waste heat, lower sensitivity to electricity prices, and quieter operation.

Table 11 presents a qualitative economic assessment of DAR and DAR-EC systems. From a CAPEX perspective, major components such as the generator and absorber are associated with moderate investment costs, while the condenser and evaporator are comparable to those of conventional refrigeration systems. The working fluids (NH_3–H_2O–inert gas) are inexpensive, and instrumentation and control requirements remain relatively simple. Thermal integration costs vary depending on site-specific conditions.

From an OPEX standpoint, DAR systems benefit from very low primary energy costs, as they operate primarily on recovered waste heat. Auxiliary electrical consumption is minimal, limited primarily to pumps and control systems. Maintenance costs are low for conventional DAR systems due to the absence of moving parts, and moderate for DAR-EC systems because of the presence of a compressor. Overall, operating costs are classified as low to medium, depending on the industrial energy context.

As shown in Table 11, the economic attractiveness of DAR and DAR-EC systems lies in the balance between moderate CAPEX and reduced OPEX. While investment costs are comparable to those of conventional refrigeration technologies, operating costs are significantly reduced due to the use of low-marginal-cost thermal energy sources, such as industrial waste heat, engine exhaust gases, or solar thermal energy.

8.2. Limitations and future work

This study proposes and analyzes two enhanced configurations of diffusion–absorption refrigeration systems. Although the results have been validated against existing literature, several limitations remain and warrant further investigation.

8.2.1. Limitations

The limitations of the present work can be classified into the following categories:

- Modelling assumptions and input data: Due to the complexity of the system, several assumptions were required to define operating conditions and simplify the modelling process. Parameters such as component efficiencies, ambient conditions, pinch-point temperature differences, and working-fluid compositions may not fully reflect real industrial environments and could be refined in future studies.
- Numerical methods: The accuracy of the results is also influenced by the numerical methods employed, including the choice of boundary conditions, discretization accuracy, rounding effects, and the use of empirical correlations. These aspects may introduce uncertainties that should be further quantified.

8.2.2. Future work

Future research should focus on improving system performance by optimizing key operating parameters such as working-fluid concentration, pressure levels, and component efficiencies. Additional studies are also needed to more ac-

curately quantify the energy-saving potential and economic benefits of integrating ejector–compressor technology into DAR systems under real industrial conditions.

Multi-objective optimization techniques represent a promising approach for simultaneously maximizing performance indicators while accounting for correlations among operating parameters. Achieving realistic and robust solutions will require identifying optimal parameter ranges rather than single operating points. Finally, future work should include transient analyses to better understand the dynamic thermophysical phenomena occurring within the system, particularly under variable industrial operating conditions.

List of symbols

A	heat transfer surface area m^2
Ex	primary exergy kJ
ex	specific exergy kJ/kg
F_i	dimensional factor –
h	specific enthalpy kJ/kg
h_i	global coefficient of heat transfer $kW/m^2.K$
$\dot{m}$	mass flow rate kg/s
$\dot{Q}$	thermal power kW
$\dot{q}_i$	exhaust gas heat transfer rate kW
s	specific entropy kJ/kg.K
T	temperature K
T_{gsor}	exit gas temperature K
ΔT	variation in temperature K
$\dot{w}$	work per time unit kJ/s
x_{NH3}	NH_3 concentration in the mixture %
η	efficiency %
ε	efficiency %

Article information

History dates
Received: 5 December 2025
Accepted: 15 February 2026
Version of record online: 21 May 2026

Notes
This paper is one of a selection of papers from CSME 2025 International Congress. École de technologie supérieure (ÉTS), Montréal (QC), May 25-28, 2025.

Copyright
© 2026 The Authors. This work is licensed under a Creative Commons Attribution 4.0 International License (CC BY 4.0), which permits unrestricted use, distribution, and reproduction in any medium, provided the original author(s) and source are credited.

Data availability
The original contributions presented in the study are included in the article, further inquiries can be directed to the corresponding author.

Author information

Author ORCIDs
Adrian Ilinca https://orcid.org/0000-0002-8236-2317

Author contributions
Conceptualization: BRMB, MTM, LMM, DRR, AI
Data curation: MTM, LMM
Formal analysis: BRMB, LMM
Funding acquisition: DRR
Investigation: BRMB, MTM, LMM, DRR, AI
Methodology: BRMB, MTM, LMM, AI
Project administration: DRR, AI
Software: BRMB, MTM, LMM
Supervision: DRR, AI
Validation: BRMB, MTM, LMM, AI
Visualization: MTM, LMM
Writing – original draft: BRMB, DRR, AI
Writing – review & editing: DRR, AI

Competing interests
The authors declare no conflicts of interest.

Funding information
Government of Canada > Natural Sciences and Engineering Research Council of Canada
RGPIN-2025-04831.

References

Adjibade, M.I.S., Thiam, A., Awanto, C., and Azilinon, D. 2017. Experimental analysis of diffusion absorption refrigerator driven by electrical heater and engine exhaust gas. Case Studies Therm. Eng. **10**: 255–261. doi:10.1016/j.csite.2017.07.004.

Alcântara, S.C.S., Lima, A.A.S., Ochoa, A.A.V., Leite, G. de N.P., Costa, J.Â.P., dos Santos, C.A.C., et al. 2022. Implementation of the characteristic equation method in quasi-dynamic simulation of absorption chillers: modeling, validation and first results. Energy Convers. Manage. X, **13**: 100165. doi:10.1016/j.ecmx.2021.100165.

Al-Hamed, K.H.M., and Dincer, I. 2019. Investigation of a concentrated solar-geothermal integrated system with a combined ejector-absorption refrigeration cycle for a small community. Int. J. Refrig. **106**: 407–426. doi:10.1016/j.ijrefrig.2019.06.026.

An, Y., Feng, B., Li, M., Gao, X., Wang, H., and Li, J. 2025. Research on peak-valley optimization of distributed photovoltaic energy storage systems based on an improved particle swarm algorithm. Int. J. Thermofluids, **30**: 101443. doi:10.1016/j.ijft.2025.101443.

Asensio-Delgado, J.M., Asensio-Delgado, S., Zarca, G., and Urtiaga, A. 2022. Analysis of hybrid compression absorption refrigeration using low-GWP HFC or HFO/ionic liquid working pairs. Int. J. Refrig. **134**: 232–241. doi:10.1016/j.ijrefrig.2021.11.013.

Asfand, F., and Bourouis, M. 2015. A review of membrane contactors applied in absorption refrigeration systems. Renewable Sustainable Energy Rev. **45**: 173–191. doi:10.1016/j.rser.2015.01.054.

Atashbozorg, D., Arasteh, A.M., Salehi, G., and Azad, M.T. 2022. Analysis of different organic rankine and kalina cycles for waste heat recovery in the iron and steel industry. ACS Omega, **7**(50): 46099–46117. doi:10.1021/acsomega.2c03922. PMID: 36570319

Aziz, M., Juangsa, F.B., Irhamna, A.R., Irsyad, A.R., Hariana, H., and Darmawan, A. 2023. Ammonia utilization technology for thermal power generation: a review. J. Energy Inst. **111**: 101365. doi:10.1016/j.joei.2023.101365.

Cefarin, M. 2015. Design of NH3-H2O absorption chiller for low grade waste heat recovery. Università degli Studi di Udine.

Trans. Can. Soc. Mech. Eng. Downloaded from cdnsciencepub.com by Ecole de technologie superieure on 09/25/26

Trans. Can. Soc. Mech. Eng. Downloaded from cdnsciencepub.com by Ecole de technologie superieure on 09/25/26

Chen, X., Omer, S., Worall, M., and Riffat, S. 2013. Recent developments in ejector refrigeration technologies. Renewable Sustainable Energy Rev. **19**: 629–651. doi:10.1016/j.rser.2012.11.028.

Chen, Y., Han, W., and Jin, H. 2016. Analysis of an absorption/absorption–compression refrigeration system for heat sources with large temperature change. Energy Convers. Manage. **113**: 153–164. doi:10.1016/j.enconman.2016.01.063.

Cheng, H., Zhang, X., Yang, P., Ding, B., and Sun, Z. 2025. Scheduling optimization of a regionally integrated energy system based on an improved multi-objective particle swarm algorithm. Energy Rep. **14**: 3888–3904. doi:10.1016/j.egyr.2025.11.022.

Chua, H.T., Toh, H.K., and Ng, K.C. 2002. Thermodynamic modeling of an ammonia–water absorption chiller. Int. J. Refrig. **25**(7): 896–906. doi:10.1016/S0140-7007(01)00101-3.

Dennis, M., and Garzoli, K. 2011. Use of variable geometry ejector with cold store to achieve high solar fraction for solar cooling. Ejector Technol. **34**(7): 1626–1632. doi:10.1016/j.ijrefrig.2010.08.006.

Dhahi Gharir, A., and Farshi, L.G. 2023. Proposal of a double ejector-two flash tank absorption refrigeration cycle: Energy, exergy and thermoeconomic evaluation. Case Stud. Therm. Eng. **50**: 103498. doi:10.1016/j.csite.2023.103498.

Dhindsa, G.S. 2021. Review on performance enhancement of solar absorption refrigeration system using various designs and phase change materials. Mater. Today: Proc. **37**: 3332–3337. doi:10.1016/j.matpr.2020.09.125.

Ezgi, C., and Bayrak, S. 2020. Experimental analysis of a laboratory-scale diesel engine exhaust heat-driven absorption refrigeration system as a model for naval surface ship applications. J. Ship Prod. Design, **36**(02): 152–159. doi:10.5957/jspd.2020.36.2.152.

Fazeli, A., Zandi, S., Golbaten Mofrad, K., Salehi, G., Khoshgoftar Manesh, M.H., and Shirmohammadi, R. 2022. Comparative thermoeconomic optimization and exergoenvironmental analysis of an ejector refrigeration cycle integrated with a cogeneration system utilizing waste exhaust heat recovery. Environ. Prog. Sustainable Energy, **41**(6): e13875. doi:10.1002/ep.13875.

Freeman, J., and Markides, C.N. 2024a. A solar diffusion-absorption refrigeration system for off-grid cold-chain provision. Part I: model development and experimental calibration. Renewable Energy, **230**: 120718. doi:10.1016/j.renene.2024.120718.

Freeman, J., and Markides, C.N. 2024b. A solar diffusion-absorption refrigeration system for off-grid cold-chain provision, Part II: system simulation and assessment of performance. Renewable Energy, **230**: 120717. doi:10.1016/j.renene.2024.120717.

Garma, R., Ben-Ezzine, N., and Bellagi, A. 2025. Experimental and numerical investigation on diffusion-absorption refrigeration system using low GWP refrigerant R600, C9H20 and helium. Int. J. Thermofluids, **27**: 101246. doi:10.1016/j.ijft.2025.101246.

Garousi Farshi, L., Seyed Mahmoudi, S.M., and Rosen, M.A. 2011. Analysis of crystallization risk in double effect absorption refrigeration systems. Appl. Therm. Eng. **31**(10): 1712–1717. doi:10.1016/j.applthermaleng.2011.02.013.

Han, W., Chen, Q., Sun, L., Ma, S., Zhao, T., Zheng, D., and Jin, H. 2014. Experimental studies on a combined refrigeration/power generation system activated by low-grade heat. Energy, **74**: 59–66. doi:10.1016/j.energy.2014.02.097.

Harraz, A.A., Freeman, J., Wang, K., Dowell, N.M., and Markides, C.N. 2019. Diffusion-absorption refrigeration cycle simulations in gPROMS using SAFT-γ Mie. Innovative Sol. Energy Trans. **158**: 2360–2365. doi:10.1016/j.egypro.2019.01.284.

Harraz, A.A., Haslam, A.J., Dowell, N.M., and Markides, C.N. 2025. Computer-aided molecular design of diffusion–absorption refrigeration modules for low-temperature solar collectors. Energy Convers. Manage. **343**: 120067. doi:10.1016/j.enconman.2025.120067.

He, H., Wang, L., Yuan, J., Wang, Z., Fu, W., and Liang, K. 2019. Performance evaluation of solar absorption-compression cascade refrigeration system with an integrated air-cooled compression cycle. Energy Convers. Manage. **201**: 112153. doi:10.1016/j.enconman.2019.112153.

Hu, Z., Deng, Z., Gao, W., and Chen, Y. 2023. Experimental study of the absorption refrigeration using ocean thermal energy and its underlying prospects. Renewable Energy, **213**: 47–62. doi:10.1016/j.renene.2023.05.086.

Jiang, W., Song, J., Jia, T., Yang, L., Li, S., Li, Y., and Du, K. 2022. A comprehensive review on the pre-research of nanofluids in absorption refrigeration systems. Energy Rep. **8**: 3437–3464. doi:10.1016/j.egyr.2022.02.087.

Karamangil, M.I., Coskun, S., Kaynakli, O., and Yamankaradeniz, N. 2010. A simulation study of performance evaluation of single-stage absorption refrigeration system using conventional working fluids and alternatives. Renewable Sustainable Energy Rev. **14**(7): 1969–1978. doi:10.1016/j.rser.2010.04.008.

Kayes, I., Nabil, M.H., Ehsan, M.M., Habib, M.A., and Khan, Y. 2025. Advanced exergy analysis and machine learning based multi-objective optimization of a modified triple cascade refrigeration system for enhanced performance. Appl. Therm. Eng. **274**: 126661. doi:10.1016/j.applthermaleng.2025.126661.

Kayes, I., Ratul, R.E., Abid, A., Majmader, F.B., Khan, Y., and Ehsan, M.M. 2024. Multi-objective optimization and 4E (energy, exergy, economy, environmental impact) analysis of a triple cascade refrigeration system. Heliyon, **10**(11): e31655. doi:10.1016/j.heliyon.2024.e31655. PMID: 38845952

Khalili, S., and Garousi Farshi, L. 2020. Design and performance evaluation of a double ejector boosted multi-pressure level absorption cycle for refrigeration. Sustainable Energy Technol. Assess. **42**: 100836. doi:10.1016/j.seta.2020.100836.

Khan, T.E., Sakib, S.H., Sakib, N., Hossain, T., Ehsan, M.M., and Khan, Y. 2025. Multi-objective optimization of a cascaded supercritical CO2 brayton cycle with ejector-enhanced transcritical CO2 and flash tank absorption refrigeration cycles. Energy Convers. Manage. X, **26**: 100988. doi:10.1016/j.ecmx.2025.100988.

Khan, Y., Faruque, M.W., Nabil, M.H., and Ehsan, M.M. 2023. Ejector and vapor injection enhanced novel compression-absorption cascade refrigeration systems: a thermodynamic parametric and refrigerant analysis. Energy Convers. Manage. **289**: 117190. doi:10.1016/j.enconman.2023.117190.

Khan, Y., Naqib Ul Islam, S.M., and Monjurul Ehsan, M. 2024a. Performance evaluation of novel advanced recompression absorption refrigeration systems equipped with ejector and vapor injection technology. Therm. Sci. Eng. Prog. **53**: 102773. doi:10.1016/j.tsep.2024.102773.

Khan, Y., Naqib-Ul-Islam, S.M., Faruque, M.W., and Ehsan, M.M. 2024b. Advanced cascaded recompression absorption system equipped with ejector and vapor-injection enhanced vapor compression refrigeration system: ann based multi-objective optimization. Therm. Sci. Eng. Prog. **49**: 102485. doi:10.1016/j.tsep.2024.102485.

Kumar, A., and Modi, A. 2024. Thermodynamic and economic evaluation of a non-cascaded dual-temperature compression–absorption–resorption refrigeration system. Appl. Therm. Eng. **236**: 121638. doi:10.1016/j.applthermaleng.2023.121638.

Liu, D., Yuan, L., Chun, L., Gong, G., Fang, X., Wang, H., et al. 2023. Thermodynamic performance analysis of a novel air conditioning system integrating solar absorption compression refrigeration and vacuum membrane-based dehumidification (SACV). Energy Build. **288**: 113021. doi:10.1016/j.enbuild.2023.113021.

Long, Z., Luo, Y., Li, H., Bu, X., and Ma, W. 2013. Performance analysis of a diffusion absorption refrigeration cycle working with TFE–TEGDME mixture. Energy Build. **58**: 86–92. doi:10.1016/j.enbuild.2012.12.003.

Lounissi, D., Bouaziz, N., and Ganaoui, M. 2017. Energetic and exergetic analysis of a novel mixture for an absorption/compression refrigeration system: R245fa/DMAC. Materials & Energy I (2015), **139**: 288–293. doi:10.1016/j.egypro.2017.11.210.

Majdi, H.S.h. 2016. Performance evaluation of combined ejector LiBr/H2O absorption cooling cycle. Case Stud. Therm. Eng. **7**: 25–35. doi:10.1016/j.csite.2016.01.003.

Mansouri, R., Bourouis, M., and Bellagi, A. 2017. Experimental investigations and modelling of a small capacity diffusion-absorption refrigerator in dynamic mode. Appl. Therm. Eng. **113**: 653–662. doi:10.1016/j.applthermaleng.2016.11.078.

Mazouz, S., Mansouri, R., and Bellagi, A. 2014. Experimental and thermodynamic investigation of an ammonia/water diffusion absorption machine. Int. J. Refrig. **45**: 83–91. doi:10.1016/j.ijrefrig.2014.06.002.

Mehr, A.S., Zare, V., and Mahmoudi, S.M.S. 2013. Standard GAX versus hybrid GAX absorption refrigeration cycle: From the view point of thermoeconomics. Energy Convers. Manage. **76**: 68–82. doi:10.1016/j.enconman.2013.07.016.

Mofrad, K.G., Zandi, S., and Salehi, G. 2023. Exergoeconomic and exergoenvironmental assessment of a geothermal-driven cogeneration

Trans. Can. Soc. Mech. Eng. Downloaded from cdnsciencepub.com by Ecole de technologie superieure on 09/25/26

system utilizing dual-pressure organic Rankine cycle and zeotropic mixtures. Energy Rep. **9**: 5206–5223. doi:10.1016/j.egyr.2023.04.271.

Mohtaram, S., Wu, W., Garcia Castellanos, H., Aryanfar, Y., Al Mesfer, M.K., Danish, M., and Irshad, K. 2023. Enhancing energy efficiency and sustainability in ejector expansion transcritical CO2 and lithium bromide water vapour absorption refrigeration systems. Therm. Sci. Eng. Prog. **43**: 101983. doi:10.1016/j.tsep.2023.101983.

Mungyeko Bisulandu, B.-J.R., Mansouri, R., and Ilinca, A. 2023. Diffusion absorption refrigeration systems: an overview of thermal mechanisms and models. Energies, **16**(9): 3610. doi:10.3390/en16093610.

Mungyeko Bisulandu, B.-J.R., Mansouri, R., Tsimba Mboko, M., Mbozi Mbozi, L., and Ilinca, A. 2024. Innovative multigeneration system with heat exchangers for harnessing thermal energy from cement kiln exhaust gases. Energies, **17**(12): 3041. doi:10.3390/en17123041.

Nabil, M.H., Khan, Y., Faruque, M.W., and Ehsan, M.M. 2023. Thermo-economic assessment of advanced triple cascade refrigeration system incorporating a flash tank and suction line heat exchanger. Energy Convers. Manage. **295**: 117630. doi:10.1016/j.enconman.2023.117630.

Papadopoulos, A.I., Kyriakides, A.-S., Seferlis, P., and Hassan, I. 2019. Absorption refrigeration processes with organic working fluid mixtures- a review. Renewable Sustainable Energy Rev. **109**: 239–270. doi:10.1016/j.rser.2019.04.016.

Peng, Z., Li, Z., Zeng, J., Yu, J., and Lv, S. 2022. Thermo-economic analysis of absorption-compression hybrid cooling systems with parallel subcooling and recooling for small scale low-grade heat source and low temperature application. Int. J. Refrig. **138**. doi:10.1016/j.ijrefrig.2022.03.003.

Pu, H., Zeng, Q., Song, T., Schonfeld, P., Wang, G., Li, W., et al. 2026. A hybrid proximal policy optimization and particle swarm algorithm for highway alignment optimization. Adv. Eng. Inf. **69**: 103959. doi:10.1016/j.aei.2025.103959.

Rady, M., Aljahdli, M., Abuhabaya, A., Almatrafi, E., Al Batati, F., and Attar, A. 2025. Experimental analysis and performance evaluation of a solar PV-driven diffusion absorption refrigeration system. Case Stud. Therm. Eng. **66**: 105754. doi:10.1016/j.csite.2025.105754.

Rattner, A.S., and Garimella, S. 2016a. Low-source-temperature diffusion absorption refrigeration. Part I: Modeling and cycle analysis. Int. J. Refrig. **65**: 287–311. doi:10.1016/j.ijrefrig.2015.10.010.

Rattner, A.S., and Garimella, S. 2016b. Low-source-temperature diffusion absorption refrigeration. Part II: Experiments and model assessment. Int. J. Refrig. **65**: 312–329. doi:10.1016/j.ijrefrig.2015.11.016.

Sanaye, S., and Refahi, A. 2020. A novel configuration of ejector refrigeration cycle coupled with organic Rankine cycle for transformer and space cooling applications. Int. J. Refrig. **115**: 191–208. doi:10.1016/j.ijrefrig.2020.02.005.

SCFP. 2019. L'ammoniac. Scfp.Ca. Available from https://scfp.ca/lammoniac#:~:text=L'ammoniac%20est%20corrosif%20pour,ammoniac%20lib%C3%A9r%C3%A9%20dans%20l'atmosph%C3%A8re [accessed March, 2025].

Shanmugam, S.K.G., and Mital, M. 2019. An ultra-low ammonia charge system for industrial refrigeration. Int. J. Refrig. **107**: 344–354. doi:10.1016/j.ijrefrig.2019.07.006.

Siddique, S.M., Muhtasim Uzzaman, M., Monjurul Ehsan, M., and Khan, Y. 2025. Thermal analysis of a novel configuration of double effect absorption system cascaded with ejector and injection enhanced compression refrigeration cycle. Energy Convers. Manage. **326**: 119435. doi:10.1016/j.enconman.2024.119435.

Starace, G., and De Pascalis, L. 2013. An enhanced model for the design of diffusion absorption refrigerators. Int. J. Refrig. **36**(5): 1495–1503. doi:10.1016/j.ijrefrig.2013.02.016.

Van Nguyen, V., Varga, S., Soares, J., Dvorak, V., and Oliveira, A.C. 2020. Applying a variable geometry ejector in a solar ejector refrigeration system. Int. J. Refrig. **113**: 187–195. doi:10.1016/j.ijrefrig.2020.01.018.

Vereda, C., Ventas, R., Lecuona, A., and Venegas, M. 2012. Study of an ejector-absorption refrigeration cycle with an adaptable ejector nozzle for different working conditions. *In* Energy solutions for a sustainable world—proceedings of the third international conference on applied energy. Vol. 97. May 16-18, 2011 - Perugia, Italy. pp. 305–312. doi:10.1016/j.apenergy.2011.12.070.

Walid Faruque, M., Khan, Y., Hafiz Nabil, M., Monjurul Ehsan, M., and Karim, A. 2023. Thermal performance evaluation of a novel ejector-injection cascade refrigeration system. Therm. Sci. Eng. Prog. **39**: 101745. doi:10.1016/j.tsep.2023.101745.

Yamamoto, E.Y., Leal Da Silva, R., and Higa, M. 2022. Performance improvements on energy and exergy basis for an ammonia-water absorption refrigeration system in a coffee industry. Sustainable Energy Technol. Assess. **52**: 102284. doi:10.1016/j.seta.2022.102284.

Yildiz, A., Ersöz, M.A., and Gözmen, B. 2014. Effect of insulation on the energy and exergy performances in diffusion absorption refrigeration (DAR) systems. Int. J. Refrig. **44**: 161–167. doi:10.1016/j.ijrefrig.2014.04.021.

Yousuf, N., Biteau, E., Anderson, T., Gschwendtner, M., and Nates, R. 2014. Modelling the performance of a diffusion absorption refrigeration system. *In* 2014-Asia-Pacific Solar Research Conference. Sydney.

Zarei, A., Zamani, J., Hooshyari, L., and Zaboli, S. 2023. Energy and exergy analysis of a novel multi-pressure levels ejector absorption-recompression refrigeration system: parametric study and optimization. Therm. Sci. Eng. Prog. **42**: 101904. doi:10.1016/j.tsep.2023.101904.

Zhang, H., Pan, X., Chen, J., and Xie, J. 2023a. Energy, exergy, economic and environmental analyses of a cascade absorption-compression refrigeration system using two-stage compression with complete intercooling. Appl. Therm. Eng. **225**: 120185. doi:10.1016/j.applthermaleng.2023.120185.

Zhang, X., Cai, L., Ma, Z., Liu, J., and Zhang, X. 2023b. Experimental investigation on single-effect and compression-assisted absorption refrigeration systems using two low-GWP HFC-based working pairs. Therm. Sci. Eng. Prog. **43**: 101999. doi:10.1016/j.tsep.2023.101999.

Zhang, K., Ma, H., Li, Q., Wang, D., Song, Q., Wang, X., and Kong, X. 2022. Thermodynamic analysis and optimization of variable effect absorption refrigeration system using multi-island genetic algorithm. Energy Rep. **8**: 5443–5454. doi:10.1016/j.egyr.2022.04.004.

Zohar, A., Jelinek, M., Levy, A., and Borde, I. 2005. Numerical investigation of a diffusion absorption refrigeration cycle. Int. J. Refrig. **28**(4): 515–525. doi:10.1016/j.ijrefrig.2004.11.003.